Univerzita Karlova v Praze

Matematicko-fyzikální fakulta

DIPLOMOVÁ PRÁCE

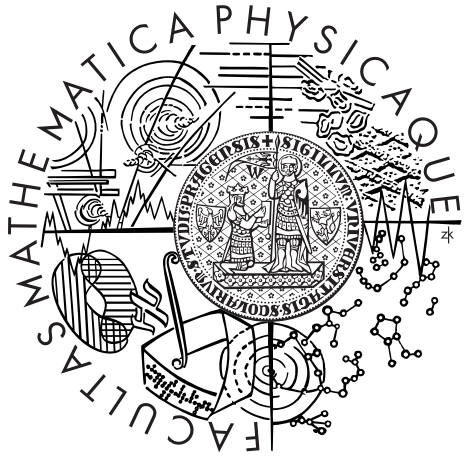

Tomáš Nosek

Studium parametrů oscilací neutrin v experimentu NOνA

Ústav částicové a jaderné fyziky

Vedoucí diplomové práce:	RNDr. Karel Soustružník, Ph.D.
Studijní program:	Fyzika
Studijní obor:	Jaderná a subjaderná fyzika

Praha 2015

Charles University in Prague

Faculty of Mathematics and Physics

MASTER THESIS

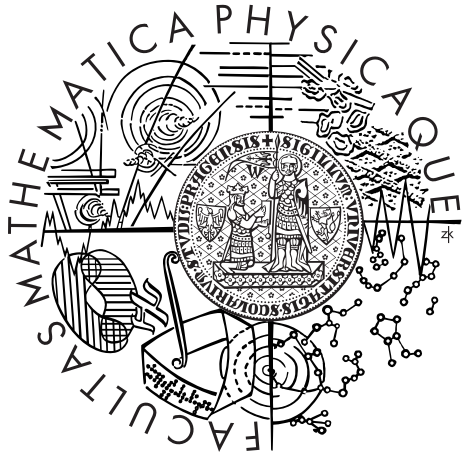

Tomáš Nosek

Study of Neutrino Oscillations Parameters at NOνA Experiment

Institute of Particle and Nuclear Physics

Supervisor of the master thesis:	RNDr. Karel Soustružník, Ph.D.
Study programme:	Physics
Specialization:	Nuclear and Subnuclear Physics

Prague 2015

I would like to thank my supervisor Karel Soustružník for the opportunity of working at the NOνA experiment. Thanks belong also to NOνA run coordinator Jaroslav Zálešák, who shared his experience and knowledge with me.

I am very grateful to Jana Nosková and Dalibor Nosek for a number of critical comments, technical suggestions, advices and help.

Finally, I would also like to thank my sister Eliška Nosková for times she takes care of me.

I declare that I carried out this master thesis independently, and only with the cited sources, literature and other professional sources.

I understand that my work relates to the rights and obligations under the Act No. 121/2000 Coll., the Copyright Act, as amended, in particular the fact that the Charles University in Prague has the right to conclude a license agreement on the use of this work as a school work pursuant to Section 60 paragraph 1 of the Copyright Act.

In ..... date ..... signature of the author

Název práce: Studium parametrů oscilací neutrin na experimentu NOνA

Autor: Tomáš Nosek

Katedra: Ústav jaderné a částicové fyziky

Vedoucí diplomové práce: RNDr. Karel Soustružník, Ph.D.

Abstrakt: Diplomová práce se zabývá fenoménem oscilací neutrin a významem experimentů s tzv. dlouhou oscilační dráhou (zejména experimentu NOνA) při měření oscilačních parametrů. Práce vychází ze standartního 3 neutrinového formalismu a seznámí čtenáře s experimentem NOνA a jeho základními fyzikálními cíli (měření směšovacích úhlů θ_{13} a θ_{23}, CP narušení, hodnota CP fáze δ a rozlišení hmotové hierarchie). Vysvětlen je vliv přítomnosti látkového prostředí na neutrinové oscilace a efektivní změna původních vakuových parametrů na nové, tzv. hmotové parametry. Práce objasňuje, jak lze využít těchto efektů hmoty v experimentech s dlouhou oscilační dráhou k určení hierarchie neutrinových hmot, a diskutuje vliv neurčitostí současných odhadů oscilačních parametrů na řešení této otázky, jinak běžně označovány také jako δ-, θ_{13}- a θ_{23}-degenerace. Poslední část práce je věnována simulaci experimentu NOνA pomocí softwaru GLoBES a výpočtu jeho citlivosti na určení hmotové hierarchie pro dvě experimentální, časově odlišné konfigurace: s tříletým během pouze v neutrinovém módu versus 1.5 roku v neutrinovém + 1.5 v antineutrinovém módu. Motivací je ukázat důležité výhody dřívějšího antineutrinového běhu oproti původně plánovanému tříletému neutrinovému zaměřujíce se přitom na problém hierarchie hmot.

Klíčová slova: neutrino, oscilace, hmotový efekt, hierarchie hmotnostních stavů, NOνA

Title: Study of Neutrino Oscillations parameters at NOνA Experiment

Author: Tomáš Nosek

Department: Institute of Particle and Nuclear Physics

Supervisor: RNDr. Karel Soustružník, Ph.D.

Abstract: This thesis aims at the neutrino oscillations phenomena and the role of long-baseline neutrino oscillation experiments and NOνA in particular in oscillation parameters search. The standard formalism of 3 neutrinos model is described, NOνA experiment and its main features and physics goals (mixing angles θ_{13} and θ_{23}, CP violation, the value of the CP phase δ and mass hierarchy determination) are introduced. The effects of media to neutrino propagation are explained and effective matter oscillation parameters are derived. The way to resolve the mass hierarchy exploiting matter effects in long-baseline neutrino oscillation experiments is depicted and consequent problems regarding the recent knowledge of oscillation parameters, i.e. δ-, θ_{13}- and θ_{23}-degeneracies, are discussed. In the last part GLoBES software is used to simulate NOνA results and to compute the estimated sensitivities to the mass hierarchy in case of 3 years ν run and 1.5ν+$1.5\bar{\nu}$ years run in order to show the advantage of an earlier switch to antineutrino mode in mass hierarchy determination.

Keywords: neutrino, oscillations, matter effect, mass hierarchy, NOνA

Contents

1. Introduction

Neutrino oscillations have become a well-established and experimentally intensively surveyed phenomenon among particle physics during the last two decades. It is now a commonly acknowledged fact, that there are at least three "flavor states" of neutrinos: $|\nu_e\rangle$ - electron, $|\nu_\mu\rangle$ - muon and $|\nu_\tau\rangle$ - tauon neutrino with defined weak charges (flavors) [1, 2], and three different "mass eigenstates": $|\nu_1\rangle$, $|\nu_2\rangle$ and $|\nu_3\rangle$ with defined masses m_1, m_2, m_3. Neutrino oscillations are paramount evidence of nonvanishing neutrino masses providing thus foremost hints about the physics beyond the Standard Model (SM).

Almost all of oscillation parameters have been measured [3]. Sizes of the mixing angles θ_{12}, θ_{13} and θ_{23} are known thanks to solar, reactor and atmospheric plus long-baseline experiments respectively, see Ref. [4]. So are the values of both mass-splittings Δm^2_{21} and Δm^2_{31} (Δm^2_{32}), also first estimates of CP violating phase δ appear [3]. The upcoming task is to aim at the last unresolved questions:

1. What is the 13-hierarchy, i.e. the sign of Δm^2_{31} (Δm^2_{32})?
2. Is 23-mixing maximal, i.e. $\theta_{23} = 45°$, and if not, is $\theta_{23} >$ or $< 45°$?
3. What is the value of CP phase δ?

These enquiries are not only motivated by the will to determine all the oscillation parameters as fundamentals, but are also essential for future theoretical progress in particle physics including extensions of the Standard Model, neutrinoless double β-decay or leptogenesis in the first moments after the Big Bang [1].

The focus of this thesis is to explain the possibility of hierarchy determination using "matter effects" in neutrino oscillations at long-baseline experiments and NOνA in detail. The first part sums up the basics of neutrino oscillations, their formalism and experimental means in oscillation parameters pursuit. Brief introduction of the NOνA experiment in USA and its important features follows. The second part is dedicated to the propagation of neutrinos through media and consequent matter effects modifying the plain vacuum oscillations. Immense attention is devoted to so-called matter resonances and their key role in mass hierarchy determination. The way to settle the particular 13(23)-hierarchy (Δm^2_{31}, Δm^2_{32}) in $\nu_\mu \to \nu_e$ channel and long-baseline experiments is comprehensively depicted. With a help of GLoBES software the last part probes the potential of NOνA in resolving neutrino mass hierarchy, especially the need of an early antineutrino run to reach some plausible results upon this topic sooner than initially expected with 3 years ν and 3 years $\bar{\nu}$ run scheduled.

The system of natural units is used throughout the text, $c = \hbar = k_B = 1$, and CPT theorem is assumed to be valid.

2. Neutrino oscillations phenomena

Chapter 2 summarizes the basic foundations of neutrino oscillations. Section 2.1 introduces standard formalism and derives vacuum transition probabilities in three neutrinos model. More on these essentials can be found in Refs. [1, 2, 5, 6, 7, 8, 9]. The importance of oscillation parameters and typical experimental designs are in scope of Section 2.2. Reader can seek for more details in Refs. [1, 2, 4, 10, 11, 12]. Short note on CP violation in neutrino oscillations is in Section 2.3, also in Refs. [1, 2, 8, 9, 13]. Section 2.4 aims at the current results in neutrino oscillation parameters search, see Ref. [3].

2.1 General formalism

A general approach towards neutrino oscillations phenomenon requires a $n > 1$ number of orthonormal neutrino flavor eigenstates $|\nu_\alpha\rangle$ of flavor α and corresponding mass eigenstates $|\nu_i\rangle$ with mass m_i. The mass eigenstates and flavor eigenstates do not coincide with one another, but are their quantum superpositions or linear combinations. Conventionally this relation is written as [1, 2, 5]

$$|\nu_\alpha\rangle = \sum_i U^*_{\alpha i}|\nu_i\rangle, \qquad |\nu_i\rangle = \sum_\alpha U_{\alpha i}|\nu_\alpha\rangle, \qquad \langle\nu_\alpha|\nu_i\rangle = U_{\alpha i}, \tag{2.1}$$

with $\langle\nu_\alpha|\nu_\beta\rangle = \delta_{\alpha\beta}$, $\langle\nu_i|\nu_j\rangle = \delta_{ij}$ and [1, 2]

$$\sum_i U_{\alpha i}U^*_{\beta i} = \delta_{\alpha\beta}, \qquad \sum_\alpha U_{\alpha i}U^*_{\alpha j} = \delta_{ij}. \tag{2.2}$$

And the coefficients $U_{\alpha i}$ form a unitary mixing matrix U.

The same relations apply to antineutrinos except for $U_{\alpha i}$ are exchanged for their complex conjugates

$$|\bar\nu_\alpha\rangle = \sum_i U_{\alpha i}|\bar\nu_i\rangle, \qquad |\bar\nu_i\rangle = \sum_\alpha U^*_{\alpha i}|\bar\nu_\alpha\rangle. \tag{2.3}$$

The $n \times n$ unitary complex matrix U has n^2 parameters. Provided neutrinos are Dirac particles, $2n-1$ physically irrelevant phases of $2n$ neutrino states can be arbitrarily fixed and $(n-1)^2$ parameters remain. If neutrinos are Majorana particles ($\nu_i = \bar\nu_i$), $(n-1)$ additional phases need to be kept, since they cannot be eliminated by phase redefinition, and the total number of free parameters is $n(n-1)$ [5].

U is a transformation matrix between $|\nu_\alpha\rangle$ and $|\nu_i\rangle$ bases. These can be treated as two independent vector representations $\nu_f \equiv (\nu_\alpha, \nu_\beta, \nu_\gamma, \ldots, \nu_\omega)^T$ (flavor representation) and $\nu_m \equiv (\nu_1, \nu_2, \nu_3, \ldots, \nu_n)^T$ (mass representation), in which a neutrino state can be expressed

$$|\nu\rangle = \sum_\alpha \nu^\alpha_f|\nu_\alpha\rangle = \sum_i \nu^i_m|\nu_i\rangle, \tag{2.4}$$

$$\langle\nu_\alpha|\nu\rangle = \nu^\alpha_f, \qquad \langle\nu_i|\nu\rangle = \nu^i_m. \tag{2.5}$$

Therefore, with Eq. (2.1)

$$\nu_f = U\nu_m. \tag{2.6}$$

2.1.1 Three neutrino mixing

So far most of the observations and experimental data are explained by a 3 neutrinos model (3ν-model) [3, 4]. Active neutrino flavors are identified through a weak interaction process of $W^\pm$ decay in which corresponding charged lepton takes part, i.e. $e \leftrightarrow \nu_e$, $\mu \leftrightarrow \nu_\mu$, $\tau \leftrightarrow \nu_\tau$.

This system of 3 flavor neutrinos $\nu_f \equiv (\nu_e, \nu_\mu, \nu_\tau)^T$ is connected with $\nu_m \equiv (\nu_1, \nu_2, \nu_3)^T$ via unitary 3×3 Pontecorvo-Maki-Nakagawa-Sakata matrix U_{PMNS}

$$\nu_f = U_{\text{PMNS}} \nu_m. \tag{2.7}$$

U_{PMNS} has 4 (6 for Majorana neutrinos) parameters: 3 mixing angles θ_{ij} and a CP violating phase δ (Majorana phases a and b). Standard parametrization of U_{PMNS} consists of three matrices of rotation $U_{ij}(\theta_{ij})$ with angles θ_{ij} in ij-planes, a diagonal $I_\delta \equiv \text{diag}(1, 1, \exp(\text{i}\delta))$ and eventual matrix of Majorana phases $A \equiv \text{diag}(\exp(\text{i}a/2), \exp(\text{i}b/2), 1)$ [1, 5, 14]

$$U_{\text{PMNS}} = \begin{pmatrix} U_{e1} & U_{e2} & U_{e3} \\ U_{\mu 1} & U_{\mu 2} & U_{\mu 3} \\ U_{\tau 1} & U_{\tau 2} & U_{\tau 3} \end{pmatrix} = U_{23}(\theta_{23}) I_\delta U_{13}(\theta_{13}) I_\delta^* U_{12}(\theta_{12}) A =$$

$$= \begin{pmatrix} 1 & & \\ & c_{23} & s_{23} \\ & -s_{23} & c_{23} \end{pmatrix} \begin{pmatrix} c_{13} & & s_{13}\text{e}^{-\text{i}\delta} \\ & 1 & \\ -s_{13}\text{e}^{+\text{i}\delta} & & c_{13} \end{pmatrix} \begin{pmatrix} c_{12} & s_{12} & \\ -s_{12} & c_{12} & \\ & & 1 \end{pmatrix} \begin{pmatrix} \text{e}^{\text{i}\frac{a}{2}} & & \\ & \text{e}^{\text{i}\frac{b}{2}} & \\ & & 1 \end{pmatrix} =$$

$$\begin{pmatrix} c_{13}c_{12} & c_{13}s_{12} & s_{13}\text{e}^{-\text{i}\delta} \\ -c_{23}s_{12} - s_{13}c_{12}s_{23}\text{e}^{+\text{i}\delta} & c_{23}c_{12} - s_{13}s_{12}s_{23}\text{e}^{+\text{i}\delta} & c_{13}s_{23} \\ s_{23}s_{12} - s_{13}c_{12}c_{23}\text{e}^{+\text{i}\delta} & -s_{23}c_{12} - s_{13}s_{12}c_{23}\text{e}^{+\text{i}\delta} & c_{13}c_{23} \end{pmatrix} \times \begin{pmatrix} \text{e}^{\text{i}\frac{a}{2}} & & \\ & \text{e}^{\text{i}\frac{b}{2}} & \\ & & 1 \end{pmatrix}, \tag{2.8}$$

with $s_{ij} \equiv \sin(\theta_{ij})$ and $c_{ij} \equiv \cos(\theta_{ij})$. The reader will see that Majorana phases a and b have no impact on neutrino oscillation probabilities. Thus from now on, let's assume the 3ν-model and drop out the matrix A from U_{PMNS}, which will be designated as U for convenience, i.e.

$$U \equiv U_{23}(\theta_{23}) I_\delta U_{13}(\theta_{13}) I_\delta^* U_{12}(\theta_{12}). \tag{2.9}$$

Note that if there are more than 3 neutrino flavors, e.g. sterile neutrinos come into play, U_{PMNS} is then just a submatrix of a larger $n \times n$ matrix and is not unitary as assumed [5].

2.1.2 Time evolution of a neutrino

The time evolution of a neutrino state $|\nu\rangle$ is given by the Schrödinger equation [1, 2, 7]

$$\begin{aligned} \text{i}\frac{\text{d}}{\text{d}t}|\nu(t)\rangle &= H|\nu(t)\rangle, & |\nu(t)\rangle &= \exp(-\text{i}Ht)\,|\nu(0)\rangle, \\ \text{i}\frac{\text{d}}{\text{d}t}\nu_m(t) &= H_m \nu_m(t), & \text{i}\frac{\text{d}}{\text{d}t}\nu_f(t) &= H_f \nu_f(t), \end{aligned} \tag{2.10}$$

where H is the Hamiltonian operator expressed in an appropriate representation basis H_m or H_f. Since mass eigenstates $|\nu_i\rangle$ are eigenstates of H with eigenvalues E_i (energy) in vacuum, one can write in a plane-wave approximation

$$|\nu_i(t)\rangle = \exp(-\text{i}Ht)\,|\nu_i(0)\rangle = \exp(-\text{i}E_i t)\,|\nu_i\rangle. \tag{2.11}$$

$E_i = m_i$ (mass of an eigenstate) and $t = \tau$ (proper time) in the rest frame of $|\nu_i\rangle$. Then through Lorentz transformation to the laboratory frame with time t, position x (distance from the source of neutrinos) and momentum p

$$|\nu_i(t)\rangle = \exp(-\text{i}(E_i t - p_i x))\,|\nu_i\rangle. \tag{2.12}$$

Assuming that neutrino is emitted at $t = 0$ with definite energy E, which means that all $|\nu_i\rangle$ have the same energy E, and being ultrarelativistic ($m_i \ll E$) [7]

$$p_i = \sqrt{E_i^2 - m_i^2} \approx E - \frac{m_i^2}{2E}, \qquad x \approx t, \tag{2.13}$$

the evolution of a mass eigenstate $|\nu_i\rangle$ is given by

$$|\nu_i(t \approx x)\rangle = \exp\left(-\mathrm{i}\frac{m_i^2}{2E}x\right)|\nu_i(0)\rangle. \tag{2.14}$$

In conclusion, the initial state $|\nu\rangle$ develops in vacuum into

$$|\nu(t \approx x)\rangle = \sum_{i=1}^{3} \exp\left(-\mathrm{i}\frac{m_i^2}{2E}x\right)|\nu_i\rangle\langle\nu_i|\nu(0)\rangle. \tag{2.15}$$

With a closer look at Eq. (2.14) and with $M^2 \equiv \mathrm{diag}(m_1^2, m_2^2, m_3^2)$ the vacuum Hamiltonian H_m in the $|\nu_i\rangle$ basis can be expressed in an effective form which happens to be very handy in investigation of neutrino oscillations

$$H_m = \frac{M^2}{2E} = \frac{1}{2E}\begin{pmatrix} m_1^2 & & \\ & m_2^2 & \\ & & m_3^2 \end{pmatrix}. \tag{2.16}$$

Schrödinger-like equation of type Eq. (2.10) then becomes

$$\mathrm{i}\frac{\mathrm{d}}{\mathrm{d}t}\nu_m = H_m\nu_m = \frac{M^2}{2E}\nu_m \tag{2.17}$$

in $|\nu_i\rangle$ basis and using mixing matrix U and H_f in flavor basis $|\nu_\alpha\rangle$

$$\mathrm{i}\frac{\mathrm{d}}{\mathrm{d}t}\nu_f = H_f\nu_f = \frac{1}{2E}UM^2U^\dagger\nu_f. \tag{2.18}$$

2.1.3 Vacuum oscillation probabilities in 3 neutrinos model

Imagine a neutrino born at the source in an eigenstate of flavor α. It travels a distance L to a detector, where it interacts with a target and produces a charged lepton of flavor β. Ipso facto, it is identified as a ν_β. From Eq. (2.1), Eq. (2.7), Eq. (2.9) and Eq. (2.15) the amplitude of such a process is [1, 6, 7]

$$\mathrm{Amp}(\nu_\alpha \to \nu_\beta; L, E) = \langle\nu_\beta|\nu_\alpha(L)\rangle = \sum_{i=1}^{3} U_{\alpha i}^* U_{\beta i} \exp\left(-\mathrm{i}\frac{m_i^2}{2E}L\right). \tag{2.19}$$

As noted earlier, this amplitude is independent of Majorana phases a and b, while

$$\sum_i (UA)_{\alpha i}^* (UA)_{\beta i} = \left(UAA^\dagger U^\dagger\right)_{\beta\alpha} = \left(UU^\dagger\right)_{\beta\alpha} = \sum_i U_{\alpha i}^* U_{\beta i}, \tag{2.20}$$

with A from Eq. (2.8).

The probability of detecting ν_β, $P(\nu_\alpha \to \nu_\beta; L)$, or the oscillation probability is given by the absolute value of amplitude from Eq. (2.19) squared:

$$\begin{aligned} P(\nu_\alpha \to \nu_\beta; L, E) &= |\mathrm{Amp}(\nu_\alpha \to \nu_\beta; L, E)|^2 = \\ &= \left|\sum_{i=1}^{3} U_{\alpha i}^* U_{\beta i} \exp\left(-\mathrm{i}\frac{m_i^2}{2E}L\right)\right|^2 = \\ &= \sum_{i=1}^{3}\sum_{j=1}^{3} U_{\alpha i}^* U_{\alpha j} U_{\beta i} U_{\beta j}^* \exp\left(-\mathrm{i}\frac{\Delta m_{ij}^2}{2E}L\right) \end{aligned} \tag{2.21}$$

with squared-mass differences (squared-mass splittings)

$$\Delta m^2_{ij} = m^2_i - m^2_j. \tag{2.22}$$

Provided CPT invariance holds, obtaining antineutrino probability is quite easy [6]:

$$P(\bar{\nu}_\alpha \to \bar{\nu}_\beta; L, E) = P(\nu_\beta \to \nu_\alpha; L, E). \tag{2.23}$$

Or, all $U_{\alpha i}$ in Eq. (2.21) need to be replaced by their complex conjugates in terms of Eq. (2.3)

$$P(\bar{\nu}_\alpha \to \bar{\nu}_\beta; L, E, U^*) = P(\nu_\alpha \to \nu_\beta; L, E, U). \tag{2.24}$$

2.2 Oscillation parameters and mass hierarchy

It can be revealed with an aid of the formula in Eq. (2.21), that vacuum neutrino oscillation probabilities in 3ν-model depend on 6 parameters: three mixing angles θ_{12}, θ_{13}, θ_{23} of mixing matrix U, CP-violating phase δ and squared-mass splittings Δm^2_{ij}, from which only two of them are independent [1, 5]. As long as this is arbitrary, one can pick Δm^2_{21} and Δm^2_{31} for instance.

Besides their absolute values also signs of squared-mass splittings are essential. Taking the masses of neutrino mass eigenstates $|\nu_i\rangle$ real they distinguish the mass ordering or mass hierachy of neutrino mass eigenstates telling us which one is the heaviest and the lightest. So far, the hierarchy of m^2_1 and m^2_2 has been resolved in oscillations of solar neutrinos with a result of $\Delta m^2_{21} > 0$[1)] [4]. On the other hand the sign of Δm^2_{31} still[2)] remains unknown leaving us with two possible mass arrangements, commonly denoted as [1, 2, 4, 5, etc.]

1. $m^2_1 < m^2_2 < m^2_3$ (normal hierarchy = NH)
2. $m^2_3 < m^2_1 < m^2_2$ (inverted hierarchy = IH).

2.2.1 The size of the squared-mass splittings importance

The physical meaning of Δm^2_{ij} emerges from $\exp\left(-\mathrm{i}\Delta m^2_{ij} L/2E\right)$ term in Eq. (2.21), which represents the periodic character of oscillation probabilities with respect to parameter L/E [1, 5, 7]. Therefore Δm^2_{ij} can be seen as an oscillation frequency in units of E/L. Or in other words, the oscillation length L_{ij} is characterized by the equation [1]

$$L_{ij} = \frac{4\pi E}{\Delta m^2_{ij}}. \tag{2.25}$$

There are only two independent Δm^2_{31}, Δm^2_{21} in 3ν-model and according to current data on neutrino oscillations (Table 2.1, Fig. 2.1) [3, 4]

$$\Delta m^2_{31} \approx \Delta m^2_{32} \approx \Delta m^2 = m^2_3 - \frac{m^2_2 + m^2_1}{2} \tag{2.26}$$

and $|\Delta m^2| \gg |\Delta m^2_{21}|$. Thanks to these odds neutrinos can be divided into two groups with two characteristic oscillation scales of L/E, where oscillation maxima/minima occur (halves of oscillation lengths) [1]. For $|\Delta m^2| = 2.5 \times 10^{-3}$ eV^2 and $\Delta m^2_{21} = 7.5 \times 10^{-5}$ eV^2 (close to current best fit values in Table 2.1):

$$\Delta m^2 \text{ scale}: \quad \frac{|\Delta m^2|}{2}\left\langle\frac{L}{E}\right\rangle \sim \pi \quad \Rightarrow \quad \left\langle\frac{L}{E}\right\rangle \approx 500\ \frac{\text{km}}{\text{GeV}} \tag{2.27}$$

$$\Delta m^2_{21} \text{ scale}: \quad \frac{|\Delta m^2_{21}|}{2}\left\langle\frac{L}{E}\right\rangle \sim \pi \quad \Rightarrow \quad \left\langle\frac{L}{E}\right\rangle \approx 16\ 000\ \frac{\text{km}}{\text{GeV}}. \tag{2.28}$$

[1)] More on the methods of hierarchy determination using matter effects in Chapters 4 and 5.

[2)] April 2015

2.2.2 The size of the mixing angles importance

With squared-mass splittings being the effective frequencies of oscillations, elements of U control the magnitudes of oscillatory patterns. They include the combinations of $\sin\theta_{ij}$ and $\cos\theta_{ij}$. Hence, the sizes of mixing angles θ_{ij} are responsible for the oscillation amplitudes. $U_{\alpha i}$ are also coefficients in linear combinations in Eq. (2.1), thus $|U_{\alpha i}|^2$ determine the relative content of $|\nu_\alpha\rangle$ in $|\nu_i\rangle$, see Fig. 2.1.

2.2.3 Some basic designs of neutrino oscillation experiments

As a result of the above subsections, neutrino oscillations are often subject to scrutiny in two basic types of experiment, for which Eq. (2.27) or Eq. (2.28) holds. The neutrino mixing can be usually[3)] treated as a mixing of 2 effective mass eigenstates in a 2ν-model in such experiments [1, 2]:

1. Atmospheric (see Refs. [4, 11]), long-baseline experiments (see Refs. [4, 12]) and reactor experiments (see Ref. [4]) at short distances (up to ~ 5 km), where Eq. (2.27) holds, are sensitive to oscillations due to Δm^2 ($\Delta m^2_{31}, \Delta m^2_{32}$). The 2ν-like oscillation probability is [1]

$$P^{2\nu}(\nu_\alpha \to \nu_\beta; L, E) = \sin^2 2\theta^{\text{eff}}_{\alpha\beta} \sin^2\left(\frac{\Delta m^2}{4E} L\right) \tag{2.29}$$

for appearance experiments and

$$P^{2\nu}(\nu_\alpha \to \nu_\alpha; L, E) = 1 - \sin^2 2\theta^{\text{eff}}_{\alpha\alpha} \sin^2\left(\frac{\Delta m^2}{4E} L\right) \tag{2.30}$$

for disappearance experiments with

$$\sin^2 2\theta^{\text{eff}}_{\alpha\beta} = 4|U_{\alpha 3}|^2|U_{\beta 3}|^2 \quad (\alpha \neq \beta), \qquad \sin^2 2\theta^{\text{eff}}_{\alpha\alpha} = 4|U_{\alpha 3}|^2\left(1 - |U_{\alpha 3}|^2\right). \tag{2.31}$$

From Eq. (2.31) and Eq. (2.8) follows that oscillation probabilities in Eq. (2.29) and Eq. (2.30) depend only on θ_{13} and θ_{23} and are independent of θ_{12}.

Atmospheric neutrinos are created in hadronic showers resulting from collisions of cosmic rays with nuclei in the atmosphere (ν_μ, ν_e mostly) [11]. Such neutrinos have energies up to hundreds of GeV and travel distances of km to thousands km depending on the arrival direction into the detector. Super-Kamiokande, SNO, IceCube or MINOS experiments are fitted to measure fluxes of neutrinos born in the atmosphere [4, 11].

Long-baseline experiments are designed to search for ν_μ ($\bar{\nu}_\mu$) disappearance or transitions to ν_e, ν_τ with $\sim$ GeV energies at $\sim 100 - 1000$ km distances. Neutrino beams used by these experiments are created at accelerator complexes (like NuMI beam at Main Injector in Fermilab or CNGS beam at SPS in CERN) from π^-/π^+ (K^-/K^+) decays. Brief summary of long-baseline experiments with their baseline and neutrino approximate energy scope follows [4, 12, 15]: K2K (250 km, $0 - 8$ GeV), MINOS (735 km, $0 - 10$ GeV), OPERA (730 km, ≈ 17 GeV), T2K (295 km, $0.2 - 2.0$ GeV), NOνA (810 km, ≈ 2.0 GeV) and a future experiment of LBNF/DUNE (formally known as LBNE) (1300 km, $0 - 10$ GeV).

Reactor experiments at short distances study disappearance of $\bar{\nu}_e$ from interactions in the nuclear reactors at $\sim$ MeV energies. They are suitable to high precision measurements of θ_{13}. Daya Bay, Double Chooz, RENO [4] are subsumed in this group of experiments.

[3)] Except for CP and T violation effects.

Table 2.1: Current best estimates of 3ν-model oscillation parameters from global fits of oscillation data [3, p. 252]. Δm^2 defined as: $\Delta m^2 = m_3^2 - (m_2^2 + m_1^2)/2$. Thus $\Delta m^2 > 0$ in case of normal hierarchy and < 0 in case of inverted hierarchy. $\sin^2\theta_{23}$ from the lower θ_{23} octant, i.e. for $\theta_{23}^{\rm HO} > 45^\circ$ $\sin^2\theta_{23}^{\rm HO} = 1 - \sin^2\theta_{23}$.

	best fit ($\pm 1\sigma$)	
parameter	$\Delta m^2 > 0$	$\Delta m^2 < 0$
$\sin^2\theta_{12}$	0.308 ± 0.017	
$\sin^2\theta_{23}$	$0.437^{+0.033}_{-0.023}$	$0.455^{+0.039}_{-0.031}$
$\sin^2\theta_{13}$	$0.0234^{+0.0020}_{-0.0019}$	$0.0240^{+0.0019}_{-0.0022}$
Δm^2_{21} $[10^{-5}$ eV$^2]$	$7.54^{+0.26}_{-0.22}$	
$\lvert\Delta m^2\rvert$ $[10^{-3}$ eV$^2]$	2.43 ± 0.06	2.38 ± 0.06
δ/π	$1.39^{+0.38}_{-0.27}$	$1.31^{+0.29}_{-0.33}$

2. Solar (see Refs. [4, 10]) and reactor experiments at long distances ($\sim$ 100 km), where Eq. (2.28) is valid, are sensitive to oscillations due to Δm^2_{21}. The effective 2ν survival probabilities are given by [1]

$$P^{2\nu}(\nu_\alpha \to \nu_\alpha; L, E) = 1 - \sin^2 2\theta^{\rm eff}_{\alpha\alpha} \sin^2\left(\frac{\Delta m^2_{21}}{4E} L\right) \tag{2.32}$$

with the mixing angle

$$\sin^2 2\theta^{\rm eff}_{\alpha\alpha} = 4\frac{|U_{\alpha 1}|^2 |U_{\alpha 2}|^2}{\left(|U_{\alpha 1}|^2 + |U_{\alpha 2}|^2\right)^2}. \tag{2.33}$$

Both solar and reactor long distance experiments measure in disappearance channels. Solar neutrinos are created in thermonuclear interactions that power the Sun and have energies of $0.1 - 20.0$ MeV and travel all the way from inside the Sun to the Earth. Solar experiments such as SAGE, GALLEX, Super-Kamiokande, SNO reported a deficit in ν_e fluxes with respect to the Standard Solar Model (SSM) [10] and determined θ_{12} and Δm^2_{21}. Thanks to the effects of matter in neutrino oscillations and total flavor transitions known as the MSW (Mikheev-Smirnow-Wolfenstein) effect [1, 2, 10, 16] the 12-hierarchy has been resolved in these experiments.

There is one delegate of reactor experiments at long distance: KamLAND. KamLAND measures $\bar\nu_e$ disappearance with a baseline of $\sim$ 175 km which resulted in the most precise determination of Δm^2_{21} [4, 10].

2.3 Charge-parity and time violation

Unlike effective 2ν-models mentioned in preceding paragraphs CP and T violation is a genuine three (or more) flavors effect. Consider the difference between appearance probability of ν_β and $\bar\nu_\beta$ for an initial ν_α and $\bar\nu_\alpha$ (CP difference) and a probability difference between T-mirror processes ($\nu_\alpha \to \nu_\beta$ and $\nu_\beta \to \nu_\alpha$, T difference)

$$\Delta P^{\rm CP}_{\alpha\beta} = P(\nu_\alpha \to \nu_\beta) - P(\bar\nu_\alpha \to \bar\nu_\beta), \qquad \Delta P^{\rm T}_{\alpha\beta} = P(\nu_\alpha \to \nu_\beta) - P(\nu_\beta \to \nu_\alpha). \tag{2.34}$$

From CPT theorem one has in vacuum

$$\Delta P^{\rm CP}_{\alpha\beta} = \Delta P^{\rm T}_{\alpha\beta}, \qquad \Delta P^{\rm CP}_{\alpha\alpha} = \Delta P^{\rm T}_{\alpha\alpha} = 0 \tag{2.35}$$

and the disappearance channels are not affected by possible CP and T violation.

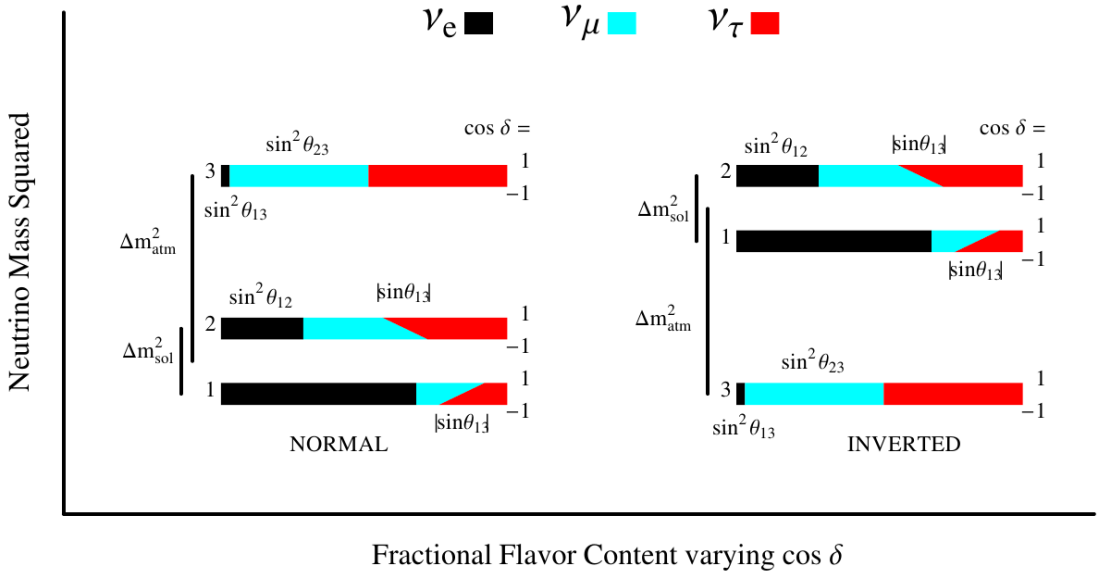

Figure 2.1: Flavor content of neutrino mass eigenstates with dependence on the Dirac phase δ. Fraction of flavor eigenstates (ν_e black, ν_μ light blue, ν_τ red) is determined by $|U_{\alpha i}|^2$. **Left:** Normal mass ordering. **Right:** Inverted mass ordering. The figure was taken from Ref. [13].

There is only one CP-violating phase δ in 3ν-model, hence only one CP (T) probability difference occurs [8]

$$\Delta P^{CP}_{e\mu} = \Delta P^{CP}_{\mu\tau} = \Delta P^{CP}_{\tau e} = \Delta P^{CP} \tag{2.36}$$

and from Eq. (2.21)

$$\begin{aligned}\Delta P^{\mathrm{CP}} &= -4 s_{12}c_{12}s_{13}c_{13}^2 s_{23}c_{23}\sin\delta\left[\sin\left(\frac{\Delta m^2_{12}}{2E}L\right)+\sin\left(\frac{\Delta m^2_{23}}{2E}L\right)+\sin\left(\frac{\Delta m^2_{31}}{2E}L\right)\right] \\ &= 2\cos\theta_{13}\sin 2\theta_{13}\sin 2\theta_{12}\sin 2\theta_{23}\sin\delta\sin\left(\frac{\Delta m^2_{21}}{4E}L\right)\sin\left(\frac{\Delta m^2_{31}}{4E}L\right)\sin\left(\frac{\Delta m^2_{32}}{4E}L\right).\end{aligned} \tag{2.37}$$

CP violation can be observed only if there is an interference between at least two different mass splittings and three mixing angles [13]. ΔP^{CP} vanishes if one $\Delta m^2_{ij} = 0$ or one $\theta_{ij} = 0$ or 90° or $\delta = 0$ or π (180°).

2.4 Current knowledge of oscillation parameters

Reader can find the best fit of oscillation parameters known up to this date in Table 2.1. The numbers are taken from Ref. [3]. In addition to it, some of the recent results from neutrino oscillation experiments that relate to the next chapters of this thesis shall be noted.

One of the most precise values of the mixing angle θ_{13} comes from the Daya Bay experiment in China. Daya Bay measures antineutrino fluxes from nuclear reactors in order to search for $\bar{\nu}_e$ disappearance [17]:

$$\sin^2 2\theta^{\mathrm{DB}}_{13} = 0.084 \pm 0.005. \tag{2.38}$$

Two long-baseline experiments T2K (295 km) in Japan and MINOS (735 km) in USA measure θ_{23} and $|\Delta m^2_{32}|$ using $\nu_\mu \to \nu_\mu$ ($\bar{\nu}_\mu \to \bar{\nu}_\mu$) beams at energies $\sim$ GeV created by large accelerators. MINOS results [18]

$$\sin^2\theta^{\mathrm{MINOS}}_{23} = 0.43^{+0.16}_{-0.04} \qquad |\Delta m^2_{32}|^{\mathrm{MINOS}} = 2.34^{+0.09}_{-0.09}\times 10^{-3}\ \mathrm{eV}^2\ \text{(NH)} \tag{2.39}$$

$$\sin^2\theta^{\mathrm{MINOS}}_{23} = 0.43^{+0.19}_{-0.05} \qquad |\Delta m^2_{32}|^{\mathrm{MINOS}} = 2.37^{+0.11}_{-0.07}\times 10^{-3}\ \mathrm{eV}^2\ \text{(IH)} \tag{2.40}$$

According to the same Ref. [18] the 90% C.L. interval for θ_{23} is

$$\sin^2\theta_{23}^{\rm MINOS} = 0.37 - 0.64 \text{ (NH)}, \qquad \sin^2\theta_{23}^{\rm MINOS} = 0.36 - 0.65 \text{ (IH)}. \tag{2.41}$$

T2K results [19]

$$\sin^2\theta_{23}^{\rm T2K} = 0.514^{+0.055}_{-0.056} \qquad |\Delta m^2_{32}|^{\rm T2K} = 2.51 \pm 0.10 \times 10^{-3} \text{ eV}^2 \text{ (NH)} \tag{2.42}$$

$$\sin^2\theta_{23}^{\rm T2K} = 0.511 \pm 0.055 \qquad |\Delta m^2_{32}|^{\rm T2K} = 2.48 \pm 0.10 \times 10^{-3} \text{ eV}^2 \text{ (IH)} \tag{2.43}$$

Almost all parameters have been determined with good precision. Few last discrepancies wait for final resolution:

1. What is the sign of Δm^2, i.e. is there normal or inverted mass hierarchy?
2. Is $\theta_{23} =, > \text{ or } < 45°$?
3. What is the size of δ (at least more precise than in Table 2.1)?

3. The NOνA experiment

Chapter 3 gives elementary information on the NOνA experiment. NuMI beam used by NOνA is described in Section 3.2, details in Refs. [4, 12, 20, 21, 22]. Section 3.3 deals with the off-axis concept, its pros and cons. Reader can found more in Refs. [1, 2, 12, 20]. The NOνA Near and Far detectors are the topic of Section 3.4. More is depicted in Refs. [4, 12, 20, 21]. The last Section 3.5 provides a brief report on typical ν interactions, their backgrounds and systematics. Refs. [4, 12, 20, 22] can procure more specific enlightenment.

3.1 Introduction

NOνA (NuMI Off-axis ν_e Appearance) [4] is a second generation long-baseline neutrino oscillation experiment located in Fermilab's NuMI (Neutrinos at the Main Injector) beamline. The main feature of NOνA is its long baseline 810 km (the longest of all recent long-baseline experiments) in combination with matter effects in Earth's mantle. These modify the vacuum oscillations in $\nu_\mu \to \nu_e$ channel making it possible to determine neutrino hierarchy and CP violation.

NOνA has two detectors (Near and Far), both sitting ca 14 mrad off the axis of the NuMI beam [22]. It is scheduled to run for 3 years in neutrino mode ($\nu_\mu \to \nu_\mu, \nu_\mu \to \nu_e$) and 3 years in antineutrino mode ($\bar{\nu}_\mu \to \bar{\nu}_\mu, \bar{\nu}_\mu \to \bar{\nu}_e$). With full start of data taking in fall 2014, the end is expected at the turn of 2020 and 2021.

Under certain conditions (see next subsections and chapters) NOνA is capable of studying several aspects of neutrino oscillations [4, 21, 22]:

1. the size of θ_{13},
2. the mass ordering, i.e. the sign of Δm^2,
3. the CP violation, i.e. $\delta \neq 0$,
4. the size of θ_{23} and Δm^2 (Δm^2_{32}, Δm^2_{31})
5. the θ_{23} ambiguity, i.e. whether $\theta_{23} =, \ >$, or $< 45°$.

Other topics of physics programme at NOνA such as supernovae neutrinos, sterile neutrinos, lepton number violation etc. can be found in Refs. [20, 21, 22], theoretical foundations in Refs. [1, 2].

3.2 NuMI beam

NuMI is a ν_μ beam used by MINOS experiment (map in Fig. 3.2). Initially it worked with power of 350 kW, but further upgrades up to 700 kW and estimated 6.0×10^{20} POT/year are scheduled [12]. 120 GeV protons from the Main Injector accelerator hit the graphite target in Target Hall producing secondary pions and kaons. Either positively or negatively charged pions (kaons) are focused by two magnetic horns towards a Decay Pipe, where most of them decay via [20, 21]

$$\pi^+ \to \mu^+ + \nu_\mu, \qquad \pi^- \to \mu^- + \bar{\nu}_\mu. \tag{3.1}$$

Following Al-Fe water cooled Hadron Absorber stops all residual protons and mesons. At last, muons from pion and kaon decays are attenuated in 250 m of earth shielding between Absorber Hall and Near Detector Hall. A schematic of NuMI beamline is in Fig. 3.1.

There are some adjustables in NuMI focusing optics configuration: position of the target and second magnetic horn with respect to the first one, the horn current and polarity [12]. Position and current of the horns fix the desired neutrino energy spectrum, or its mean energy more likely. In combination with off-axis concept this has a potential to pick a neutrino energy spectrum with very sharp peak at a certain energy as it is done for NOνA (2 GeV).

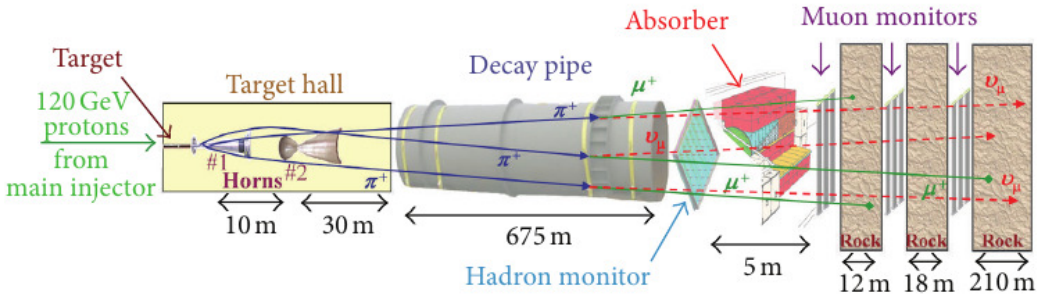

Figure 3.1: A schematic of NuMI beamline. **From left to right:** 120 GeV protons hit the carbon target in the Target Hall producing pions and kaons. These are focused by two magnetic horns, then decay while travelling through the Decay Pipe. Except for muons all produced hadrons and mesons are stopped in the Hadron Absorber. Residual muons are attenuated by nearly 250 m of rock in front of the Near Detector leaving just neutrinos in the beam. The figure was taken from Ref. [12].

Figure 3.2: Map of NuMI beamline. The figure was downloaded (2015/03/09) from: http://www-nova.fnal.gov/images_v2/graphics/numi-beamline-map-med.jpg.

The optimal setup for the NOνA experiment is so-called "medium energy tune" (Fig. 3.3 - right) (MINOS run with "low energy tune") with peak at 7.5 GeV on-axis.

By changing polarity of the horns a ν_μ or $\bar{\nu}_\mu$ beam can be chosen. To be more precise, one shall talk about ν_μ dominated and $\bar{\nu}_\mu$ enhanced beams. With the magnetic horn polarity set to focus positive hadrons (ν_μ mode) the on-axis beam consist of 91.7% ν_μ, 7.0% $\bar{\nu}_\mu$ and 1.3% $\nu_e + \bar{\nu}_e$, with the opposite polarity ($\bar{\nu}_\mu$ mode) of 40% $\bar{\nu}_\mu$, 58% ν_μ and 2% $\nu_e + \bar{\nu}_e$ [12]. Despite this fact, the NOνA off-axis detectors will see a beam flux with significantly higher purity than on-axis having 1% $\bar{\nu}_\mu$ contamination in ν_μ mode and about 5% ν_μ contamination in $\bar{\nu}_\mu$ mode.

3.3 Off-axis concept

Both of NOνA detectors are located ca 14 mrad off-axis of the NuMI beam. Appreciable outcome of the relativistic kinematics is the main reason for such a disposition. In their rest frame, pions and kaons decay isotropically producing mono-energetic neutrinos. When boosted, the energy E_ν of a neutrino from a decay of pion (kaon) Eq. (3.1) of energy E

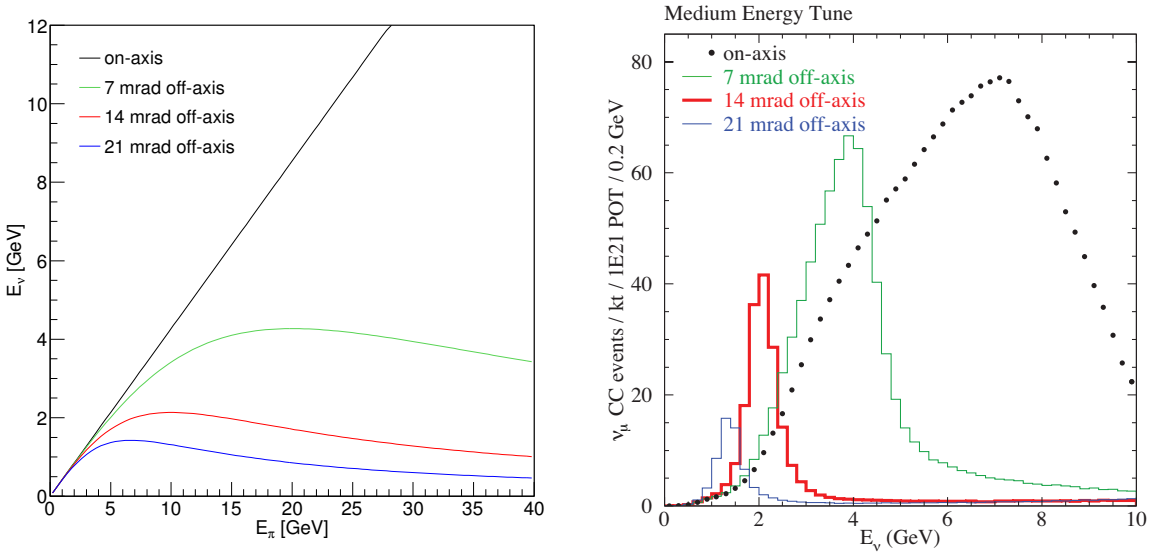

Figure 3.3: **Left:** Energy of a muon neutrino with respect to the energy of an initial pion for different off-axis angles. **Right:** The simulated NuMI off-axis beam energy spectra in "medium energy" configuration. 14 mrad off-axis (red histogram) is the case of NOνA. The figure was downloaded (2015/03/09) from: http://www-nova.fnal.gov/plots_and_figures/1400_Neutrino_Spectra/050-me-spectra.png.

at a small laboratory angle ϕ is

$$E_\nu = \frac{(1 - m_\mu^2/m^2)E}{1 + E^2\phi^2/m^2} \Leftarrow \begin{cases} \left(1 - \frac{m_\mu^2}{m_\pi^2}\right) \approx 0.427 & \text{for pions,} \\ \left(1 - \frac{m_\mu^2}{m_K^2}\right) \approx 0.954 & \text{for kaons,} \end{cases} \tag{3.2}$$

with m the mass of the initial particle and m_μ the mass of muon. For detailed derivation of Eq. (3.2) see Ref. [2, p. 66]. Unlike the energy on axis of the beam, energy of off-axis neutrinos is less dependent on the pion (kaon) energy as you can see in Fig. 3.3 - left.

Experimental off-axis layout has a number of pros and cons. The main con is a suppresion of the overall neutrino flux, because it obviously peaks in the forward direction. On the other hand, off-axis position provides extra flux in the chosen energy region and moreover effectively discriminates neutrinos with higher and lower energies. The consequent neutrino spectrum is relatively narrow and sharp, which helps to reduce backgrounds with usually much broader energy distribution (NC events) [20, 21]. Also high energy tail is lowered, τ backgrounds with a threshold slightly above 3 GeV, when ν scatters on a nucleon, are minimized [20]. Fig. 3.3 - right shows the simulated NuMI energy spectrum in on-axis beam and three off-axis directions.

A conclusion of the previous two sections emerges: peak energy of the neutrino spectrum is primarily determined by a combination of focusing optics "energy tune" and the off-axis angle. Focusing optics itself affects the on-axis beam energy and, given a certain off-axis angle, off-axis beam intensity [21]. Picking out carefully the beam power, focusing configuration, off-axis angle and sufficient baseline optimizes the experimental sensitivity to particular object of interest. The parameters of NOνA experiment ($L = 810$ km, $E \approx 2.0$ GeV) maximizes sensitivity to the mass ordering resolution and observation of CP violation effects [4].

3.4 Detectors

NOνA has two detectors: Far Detector (FD) in Ash River, Minnesota, ca 810 km from a Fermilab site and Near Detector (ND) ca 1 km from the target next to the MINOS near

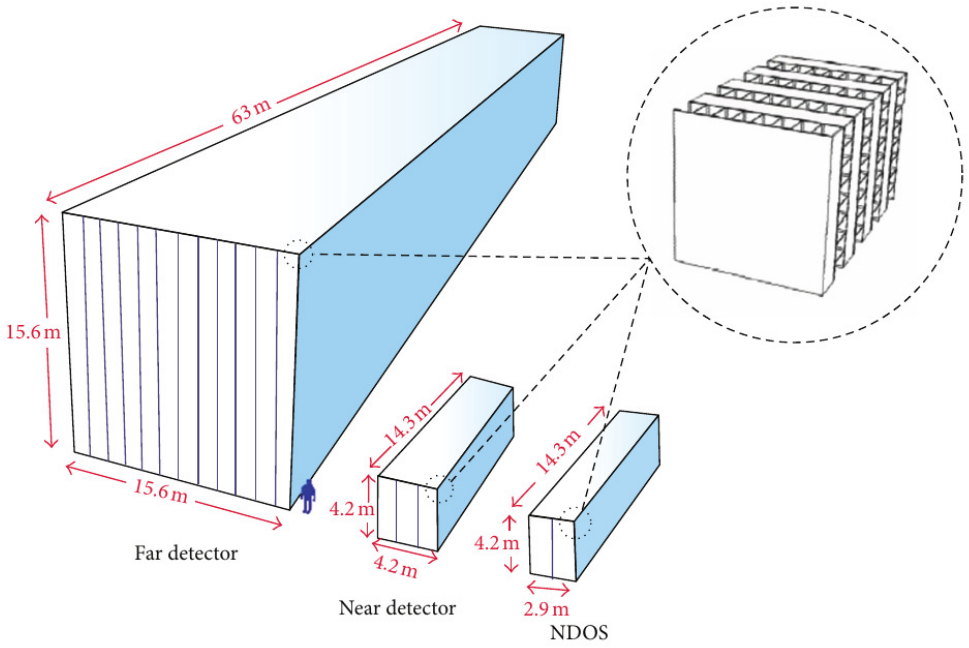

Figure 3.4: A drawing of NOνA detectors (including prototype NDOS) with a human figure for scale. **Inset:** An illustration of PVC cellular structure and detectors' high segmentation. Each layer of elementary cells is oriented orthogonally to adjacent ones to provide 3D event reconstruction. The figure was adapted from Ref. [12].

detector at Fermilab, Batavia, Illinois. The NOνA detectors are almost totally active, highly segmented, tracking liquid scintillator calorimeters. FD is constituted of approximately 11 200 metric tons of mineral-oil based liquid scintillator and 2 800 tons of highly reflective polyvinyl chloride extrusions to contain it, i.e. 14 kt of fiducial mass [12, 21]. The elementary cells of 4.5 cm $\times$ 6 cm $\times$ 15.6 m are glued together in modules of 32 cells. Twelve modules next to each other make up a plane and the planes alternate in having their long dimension horizontal and vertical. FD has 896 layers with 384 cells, i.e. $\sim$ 344 000 readout channels. ND is similar, but much smaller with total mass $\sim$ 300 t and 4.5 cm $\times$ 6 cm $\times$ 4.1 m size of elementary cells and is supplemented with a muon catcher to shorten muons stopping range. See Fig. 3.4 with drawings of NOνA detectors.

Light is emitted when a charged particle travels through the scintillator and extracted by a U-shaped wavelength-shifting fiber. Both ends of the fiber are attached to a 32-pixel avalanche photodiode (APD) [21]. APDs must be cooled to –15°C to obtain low noise on output. Detectors assembly and instrumentation was completed in September 2014.

NOνA has operated a prototype near detector on the surface since 2010 (NDOS, also in Fig. 3.4) to study interaction topologies, detector response, test detector adjusment, develop electronics and data acquisition etc. NDOS is located 110 mrad off NuMI beam axis and is very similar to ND. For more information and results achieved with NDOS see Refs. [20, 21, 23].

3.5 Interactions, backgrounds and systematics

NOνA uses CC events for $\nu_e/\bar{\nu}_e$ and $\nu_\mu/\bar{\nu}_\mu$ detection. Typical interactions to be sought in the detectors are

$$\nu_e + \text{nucleus} \to e^- + X, \qquad \nu_\mu + \text{nucleus} \to \mu^- + X. \tag{3.3}$$

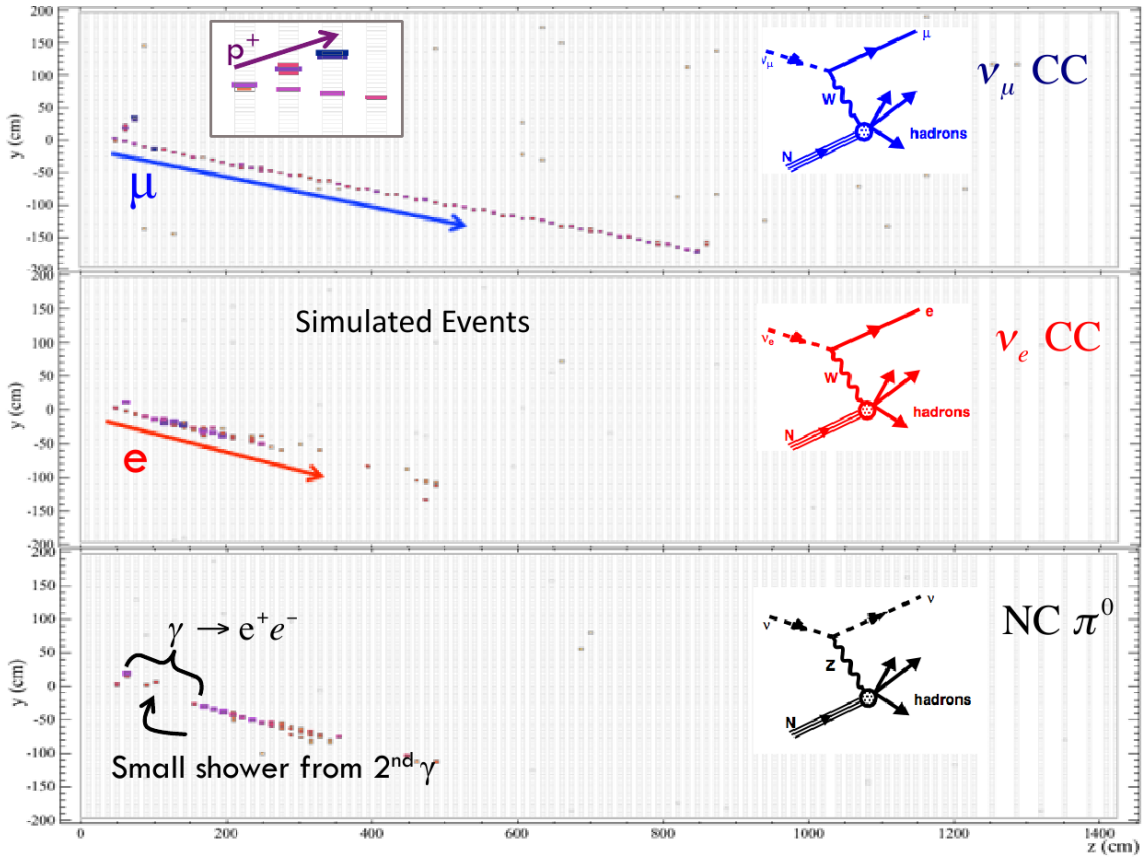

Figure 3.5: Distinguishing neutrino events in the NOνA Near Detector. Each small rectangle represents the individual elementary cells of the detector. The darker cell is the higher energy deposit was measured. **Top to bottom:** ν_μ CC quasi-elastic event with proton and characteristic muon; ν_e CC quasi-elastic event with electromagnetic shower caused by an electron; NC event with π^0 production. The figure was taken from [22].

Distinguished topologies can be seen in Fig. 3.5. The total number of $\nu_e/\bar{\nu}_e$ events expected for 3+3 years run with 6.0 $\times 10^{20}$ POT/year is 60 – 70/30 – 40 [24].

Having two detectors is a major advantage in dealing with backgrounds and systematics. ND unoscillated beam spectra, its backgrounds and subsequent extrapolation are a measure of the expected background to $\nu_\mu \rightarrow \nu_e$ oscillation signals in FD [20]. Operational and structural similarity of detectors ensures that the efficiencies for signal and background are nearly identical. However, there are some issues that one should be aware of [20]:

1. Energy resolutions of detectors are different and, as a consequence, so are their absolute energy calibrations. Energy dependent background (NC events) needs this to be understood perfectly.
2. Beam spectra cannot be identical, because ND sees a line source of muon neutrinos from decays hundreds meters away, while FD sees a point source from 810 km.
3. ND is underground and shielded from cosmic rays, while FD is on the surface. In order to reduce cosmic photons which can be misidentified as ν_e CC events FD's roof is composed of normal and barite-enhanced concrete with twelve radiation length overburden.

4. Effects of matter in neutrino oscillations

Chapter 4 explores the impact of matter on neutrino oscillations and the effective modification of oscillation parameters in 3ν-model. Sections 4.1 and 4.2 derive the scattering potentials and corresponding matter Hamiltonian, also in Refs. [1, 7, 14, 25]. Section 4.3 is dedicated to a diagonalization of this Hamiltonian in order to find relations for effective oscillation parameters. Conditions of resonances and adiabatic flavor transitions are discussed. Inspect Refs. [1, 14, 25] for details or Refs. [26, 27] for more rigorous results. Exhausting explanations of neutrino oscillations in matter phenomena concerning lots of theoretical and experimental usage are in Ref. [1] and Ref. [14].

4.1 Coherent forward scattering and matter potentials

When propagating through media, neutrinos undergo weak interactions with other particles via exchange of $W^{\pm}$ (CC) and Z^0 gauge bosons (NC) [7, 14], see Fig. 4.1. At low energies (center-of-mass energies lower than the masses of weak gauge bosons) and assuming that matter consists almost only of protons p, neutrons n and electrons e [14, 25], the interaction Hamiltonian can be expressed as an effective four-fermion Hamiltonian [14]

$$H_{\text{int}} = \frac{G_F}{\sqrt{2}} \bar{\nu}\gamma^{\mu}(1-\gamma_5)\nu \left[\bar{e}\gamma_{\mu}(g_V + g_A\gamma_5)e + \bar{p}\gamma_{\mu}(g_V^p + g_A^p\gamma_5)p + \bar{n}\gamma_{\mu}(g_V^n + g_A^n\gamma_5)n\right], \quad (4.1)$$

where G_F is the Fermi coupling constant, g_V and g_A are the vector and axial vector coupling constants respectively, γ_{μ}, γ_5 corresponding γ-matrices and ν, e, p, n stand for fermion fields.

In the Standard Model the matrix of the potentials in $|\nu_{\alpha}\rangle$ basis is diagonal (flavor states are eigenstates of weak interaciton). For the coherent forward scattering on electrons, neither ν_{μ}, nor ν_{τ} has CC contribution [25]. NC interactions, on the other hand, treat all neutrino flavors in the same manner. NC scattering potentials on electrons and protons are equal and opposite, hence they cancel each other in electrically neutral media [1, 14]. Neutrons contribute to the potential proportionally to their density. Assuming coherent forward scattering and that medium is unpolarized with zero average particle momenta, this results in an effective interaction potential [14]

$$V_{\alpha} = \sqrt{2}G_F \left(\delta_{\alpha e}N_e - \frac{1}{2}N_n\right), \quad (4.2)$$

where N_e is electron and N_n neutron density of the medium. The matrix of interaction potentials in flavor basis V_f is therefore

$$V_f = \begin{pmatrix} V_e & & \\ & V_{\mu} & \\ & & V_{\tau} \end{pmatrix} = \sqrt{2}G_F \begin{pmatrix} N_e - \frac{N_n}{2} & & \\ & -\frac{N_n}{2} & \\ & & -\frac{N_n}{2} \end{pmatrix}. \quad (4.3)$$

V_f is then added to H_f (vacuum propagation Hamiltonian in $|\nu_{\alpha}\rangle$ basis) from Eq. (2.16) to form the neutrino propagation Hamiltonian in matter $\mathcal{H}_f$.

Oscillation probabilities depend on relative phases of the different neutrino eigenstates (θ_{ij}, $\Delta m^2_{ij}, \delta$) and they cannot be affected by interaction that shifts the eigenvalues of Hamiltonian by the same amount [5, 25]. Ergo, the NC contribution (Z^0 exchange) can be left out. Or equivalently: since only the difference of potentials has a physical meaning [14],

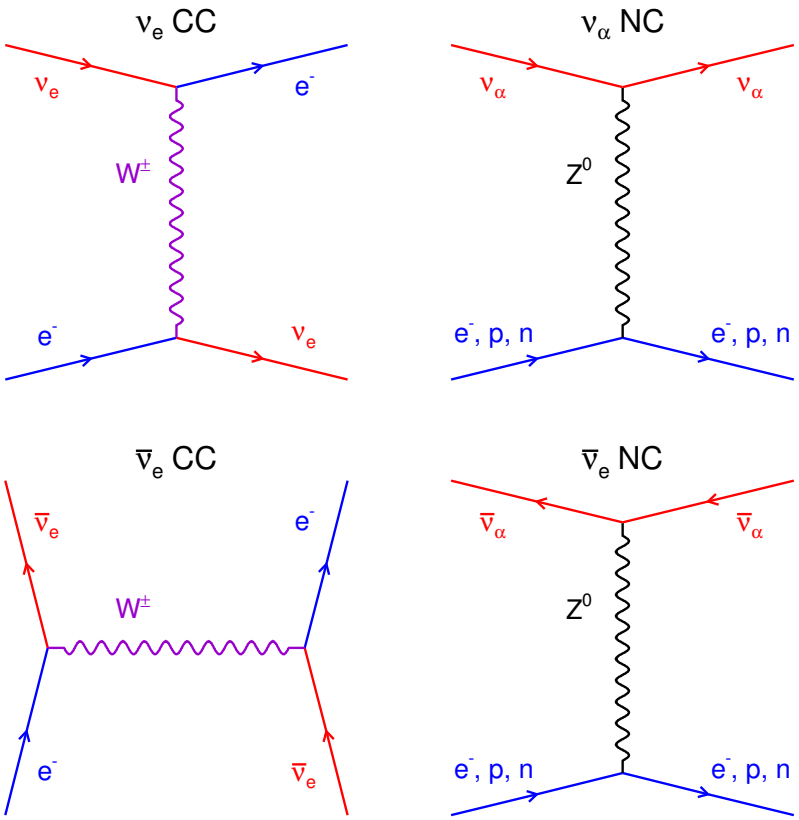

Figure 4.1: Feynmann diagrams of neutrino weak interactions in matter. **Left semi-plane:** CC interactions of $\nu_e/\bar{\nu}_e$ and e^- mediated by $W^\pm$ bosons. **Right semi-plane:** NC interactions of $\nu_\alpha/\bar{\nu}_\alpha$ and e^-, p, n mediated by Z^0 boson. **Upper semi-plane:** Neutrino interactions. **Lower semi-plane:** Interactions of antineutrinos.

the matter Hamiltonian of neutrino propagation can be written as

$$\mathcal{H}_f = H_f + V_f = H_f + \sqrt{2}G_F \begin{pmatrix} N_e - \frac{N_n}{2} & & \\ & -\frac{N_n}{2} & \\ & & -\frac{N_n}{2} \end{pmatrix} \xrightarrow{\text{eff.}} H_f + \begin{pmatrix} V & & \\ & 0 & \\ & & 0 \end{pmatrix}, \tag{4.4}$$

where V is the effective electron potential (from now on denoted simply as V for simplicity)

$$V \equiv \sqrt{2}G_F N_e. \tag{4.5}$$

The potential for antineutrinos can be formally obtained as $V \to -V$ [1, 14, 25].

4.2 Time evolution and effective Hamiltonian

As stated earlier, effective Hamiltonian $\mathcal{H}$ of oscillations in matter in flavor basis ($\mathcal{H}_f$) is a sum of vacuum Hamiltonian H_f and effective potentials V_f [1, 14]

$$\mathcal{H}_f = H_f + V_f = \frac{1}{2E} U M^2 U^\dagger + V_f = \frac{1}{2E}\left[U M^2 U^\dagger + \begin{pmatrix} 2EV & & \\ & 0 & \\ & & 0 \end{pmatrix}\right], \tag{4.6}$$

where U is the mixing matrix from Eq. (2.9) and M^2 is a diagonal matrix of masses squared from Eq. (2.16). Time evolution of an arbitrary neutrino state in matter is then given by an equation similar to Eq. (2.10)

$$\mathrm{i}\frac{\mathrm{d}}{\mathrm{d}t}|\nu(t)\rangle = \mathcal{H}|\nu(t)\rangle, \qquad |\nu(t)\rangle = \exp\left(-\mathrm{i}\mathcal{H}t\right)|\nu(0)\rangle, \tag{4.7}$$

with $\mathcal{H}$ being the matter Hamiltonian expressed in an appropriate basis.

While oscillation probabilities do not depend on absolute scales, but rather only on the differences of subjected eigenvalues [1, 14, 25, 26, 27], M^2 can be simplified in terms of $m_1^2 = 0$

$$M^2 = \begin{pmatrix} m_1^2 & & \\ & m_2^2 & \\ & & m_3^2 \end{pmatrix} \xrightarrow{\text{eff.}} \begin{pmatrix} 0 & & \\ & \Delta m_{21}^2 & \\ & & \Delta m_{31}^2 \end{pmatrix} \approx \Delta m^2 \begin{pmatrix} 0 & & \\ & a & \\ & & 1 \end{pmatrix}, \tag{4.8}$$

where

$$a \equiv \frac{\Delta m_{21}^2}{\Delta m^2}, \tag{4.9}$$

which will be focused on later due to its relatively small value ≈ 0.03 rooted in the observed strong hierarchy of the squared-mass differences ($|\Delta m^2| \gg |\Delta m_{21}^2|$).

For the neutrino mixing is defined with respect to the eigenstates of the Hamiltonian, the further task is to find the eigenstates $|N_i\rangle$ of $\mathcal{H}$, understood in a clear connection with vacuum oscillations as the effective mass eigenstates in matter [14]. Common eigenstate equation would be

$$\mathcal{H}|N_i\rangle = \mathcal{H}_i|N_i\rangle = \frac{M_i^2}{2E}|N_i\rangle \tag{4.10}$$

with $\mathcal{H}_i = M_i^2/2E$ the eigenvalues of $\mathcal{H}$, M_i^2 is the effective mass of a mass eigenstate $|N_i\rangle$. As this is, after all, only a generalization of the vacuum mixing, there has to be a matter mixing matrix $\mathcal{U}$, that relates the flavor states with the effective matter mass states in the sense of Eq. (2.7), $N \equiv (N_1, N_2, N_3)^T$,

$$\nu_f = \mathcal{U}N. \tag{4.11}$$

Or, $\mathcal{U}$ is the transformation matrix between the basis of flavor states and the basis of matter mass states, in which is the Hamiltonian diagonal. Using $\mathcal{M}^2 \equiv \text{diag}(M_1^2,\ M_2^2,\ M_3^2)$, Eq. (4.4) and Eq. (4.8), one can write

$$\begin{aligned} \mathcal{H}_f &= \mathcal{U}\mathcal{H}_m\mathcal{U}^\dagger = \frac{1}{2E}\mathcal{U}\mathcal{M}^2\mathcal{U}^\dagger = \frac{1}{2E}\mathcal{U}\begin{pmatrix} M_1^2 & & \\ & M_2^2 & \\ & & M_3^2 \end{pmatrix}\mathcal{U}^\dagger = \\ &= \frac{\Delta m^2}{2E}\left[U\begin{pmatrix} 0 & & \\ & a & \\ & & 1 \end{pmatrix}U^\dagger + \begin{pmatrix} \frac{2VE}{\Delta m^2} & & \\ & 0 & \\ & & 0 \end{pmatrix}\right], \end{aligned} \tag{4.12}$$

where $\mathcal{H}_m = \mathcal{M}^2/2E$ is the matter Hamiltonian in the basis of effective matter mass eigenstates $|N_i\rangle$.

4.3 Diagonalization of matter Hamiltonian

In order to find the eigenvalues of matter Hamiltonian $M_i^2/2E$ and effective matter mixing matrix $\mathcal{U}$, a diagonalization of $\mathcal{H}_f$ shall be performed. The exact expressions for oscillation parameters in matter are rather complicated and difficult to analyze, the reader can find them in Refs. [28, 29] if interested. More frequently, some sort of analytical approximation or numerical computations are being used. The approximative diagonalization described in next few paragraphs is similar to that in Ref. [14] and relies on the strong hierarchy of the squared-mass differences $a \approx 0.03$ from Eq. (4.9) and a relatively small value of θ_{13}. To stay as simple and comprehensible as possible, instead of explicit expressions of matter oscillation parameters with respect to vacuum parameters, formal rotation technique was used with only one effective matter angle given explicitly. Higher precision analytical calculations can be found e.g. in Refs. [26, 27].

First of all, it is convenient to make use of the following relations [26]

$$I_\delta^\dagger U_{12} I_\delta = U_{12}, \quad I_\delta^\dagger \mathrm{diag}(a,b,c) I_\delta = \mathrm{diag}(a,b,c), \quad I_\delta I_\delta^\dagger = 1, \tag{4.13}$$

where $U_{12} \equiv U_{12}(\theta_{12})$ and I_δ are from Eq. (2.8). Remind the factorization of U from Eq. (2.9) and notice that $U_{23}(\theta_{23})$ and I_δ can be permuted with V_f in Eq. (4.6), since the potential matrix is invariant under *23* rotations[1)]. Inserting Eqs. (4.13) into right places in Eq. (4.12) one gets [14, 26]

$$\mathcal{H}_f = \frac{\Delta m^2}{2E} U_{23} I_\delta \left[U_{13} U_{12} \begin{pmatrix} 0 & & \\ & a & \\ & & 1 \end{pmatrix} U_{12}^\dagger U_{13}^\dagger + \begin{pmatrix} \frac{2VE}{\Delta m^2} & & \\ & 0 & \\ & & 0 \end{pmatrix} \right] I_\delta^\dagger U_{23}^\dagger \tag{4.14}$$

with $U_{ij} \equiv U_{ij}(\theta_{ij})$ the rotational matrices in ij-planes from Eq. (2.8). The diagonalization of $\mathcal{H}_f$ will consist of four consecutive rotations of the propagation basis:

$$\mathcal{H}_f \xrightarrow{U_{23}(\theta_{23})I_\delta} \dot{\mathcal{H}} \xrightarrow{U_{13}(\Theta_{13})} \ddot{\mathcal{H}} \xrightarrow{U_{12}(\Theta_{12})} \dddot{\mathcal{H}} \xrightarrow{U_{23}(\tilde{\theta}_{23})} \mathcal{H}_m, \tag{4.15}$$

where all the rotations are again in ij-planes, but, except for the first one, with new effective angles in matter Θ_{13}, Θ_{12} and a very small $\tilde{\theta}_{23}$, which importance will be clarified later.

After the first trivial rotation (or simply omitting $U_{23}(\theta_{23})I_\delta$) the initial $\mathcal{H}_f$ becomes

$$\dot{\mathcal{H}} = \frac{\Delta m^2}{2E} \left[U_{13} U_{12} \begin{pmatrix} 0 & & \\ & a & \\ & & 1 \end{pmatrix} U_{12}^\dagger U_{13}^\dagger + \begin{pmatrix} \frac{2VE}{\Delta m^2} & & \\ & 0 & \\ & & 0 \end{pmatrix} \right] \tag{4.16}$$

or explicitly

$$\dot{\mathcal{H}} \equiv \frac{\Delta m^2}{2E} \begin{pmatrix} \dot{h}_{11} & \dot{h}_{12} & \dot{h}_{13} \\ \dot{h}_{21} & \dot{h}_{22} & \dot{h}_{23} \\ \dot{h}_{31} & \dot{h}_{32} & \dot{h}_{33} \end{pmatrix} = \frac{\Delta m^2}{2E} \begin{pmatrix} s_{13}^2 + a s_{12}^2 c_{13}^2 + \frac{2EV}{\Delta m^2} & a s_{12} c_{12} c_{13} & s_{13} c_{13} (1 - a s_{12}^2) \\ \circ & a c_{12}^2 & -a s_{12} c_{12} s_{13} \\ \circ & \circ & c_{13}^2 + a s_{12}^2 s_{13}^2 \end{pmatrix}, \tag{4.17}$$

where $s_{ij} \equiv \sin\theta_{ij}, c_{ij} \equiv \cos\theta_{ij}$ as earlier in Eq. (2.8), $\dot{h}_{ij}$ are the elements of $\dot{\mathcal{H}}$. $\dot{\mathcal{H}}$ is real and unitary, i.e. $\circ$ stands for the same terms from across the diagonal. Here all the off-diagonal elements contain small parameters a and/or s_{13}, whereof an advantage will be taken.

After the second *13* rotation

$$\dot{\mathcal{H}} = U_{13}(\Theta_{13}) \ddot{\mathcal{H}} U_{13}(\Theta_{13})^\dagger \tag{4.18}$$

over the angle Θ_{13} given by

$$\tan 2\Theta_{13} = \frac{2\dot{h}_{13}}{\dot{h}_{33} - \dot{h}_{11}} = \frac{\sin 2\theta_{13}}{\cos 2\theta_{13} - \frac{2EV}{\Delta m^2 (1 - a s_{12}^2)}} \tag{4.19}$$

the 1-3 element from Eq. (4.17) vanishes and the Hamiltonian in $|\ddot{\nu}\rangle$ basis can be written as

$$\ddot{\mathcal{H}} \equiv \frac{\Delta m^2}{2E} \begin{pmatrix} \ddot{h}_{11} & \ddot{h}_{12} & 0 \\ \ddot{h}_{21} & \ddot{h}_{22} & \ddot{h}_{23} \\ 0 & \ddot{h}_{32} & \ddot{h}_{33} \end{pmatrix} = \frac{\Delta m^2}{2E} \begin{pmatrix} \ddot{h}_{11} & a s_{12} c_{12} \cos(\Theta_{13} - \theta_{13}) & 0 \\ \circ & a c_{12}^2 & a s_{12} c_{12} \sin(\Theta_{13} - \theta_{13}) \\ 0 & \circ & \ddot{h}_{33} \end{pmatrix}, \tag{4.20}$$

[1)] Italic numbers denote the plane of rotation, e.g. *23* rotation is a rotation in a plane of the second and the third coordinate.

where

$$\begin{aligned}
\ddot{h}_{11} &= \dot{h}_{11}\cos^2\Theta_{13} + \dot{h}_{33}\sin^2\Theta_{13} - \dot{h}_{13}\sin 2\Theta_{13} = \\
&= \sin^2(\Theta_{13}+\theta_{13}) + as_{12}^2\cos^2(\Theta_{13}+\theta_{13}) + \frac{2EV}{\Delta m^2}\cos^2\Theta_{13}, \qquad (4.21)\\
\ddot{h}_{33} &= \dot{h}_{11}\sin^2\Theta_{13} + \dot{h}_{33}\cos^2\Theta_{13} + \dot{h}_{13}\sin 2\Theta_{13} = \\
&= \sin^2(\Theta_{13}-\theta_{13}) + as_{12}^2\cos^2(\Theta_{13}-\theta_{13}) + \frac{2EV}{\Delta m^2}\cos^2\Theta_{13}. \qquad (4.22)
\end{aligned}$$

Either 1-2, or 2-3 element of $\ddot{\mathcal{H}}$ in Eq. (4.20) is very small comparing to differences between diagonal elements $(\ddot{h}_{ii} - \ddot{h}_{jj})$[2)], depending on the size of Θ_{13} ($\xrightarrow{VE\to 0}$ θ_{13} or $\xrightarrow{VE\to\infty}$ $\pi/2$ or $\xrightarrow{VE\to-\infty}$ 0). Suppose for the moment, that $\ddot{h}_{23} = as_{12}c_{12}\sin(\Theta_{13}-\theta_{13})$ can be neglected and $\ddot{h}_{33}$ effectively decouples from *12* submatrix. Then the following *12* rotation

$$\ddot{\mathcal{H}} = U_{12}(\Theta_{12})\ddot{\mathcal{H}}U_{12}(\Theta_{12})^\dagger \qquad (4.23)$$

over the angle

$$\tan 2\Theta_{12} = \frac{2\ddot{h}_{12}}{\ddot{h}_{22}-\ddot{h}_{11}} = \frac{a\sin 2\theta_{12}\cos(\Theta_{13}-\theta_{13})}{a[c_{12}^2 - s_{12}^2\cos^2(\Theta_{13}+\theta_{13})] - \sin^2(\Theta_{13}+\theta_{13}) - \frac{2EV}{\Delta m^2}\cos^2\Theta_{13}}, \qquad (4.24)$$

makes the 1-2 element of $\ddot{\mathcal{H}}$ vanish. Exploiting previous denotation of matrix elements

$$\begin{aligned}
\dddot{h}_{11} &= \ddot{h}_{11}\cos^2\Theta_{12} + \ddot{h}_{22}\sin^2\Theta_{12} - \ddot{h}_{12}\sin 2\Theta_{12}, \qquad (4.25)\\
\dddot{h}_{22} &= \ddot{h}_{11}\sin^2\Theta_{12} + \ddot{h}_{22}\cos^2\Theta_{12} + \ddot{h}_{12}\sin 2\Theta_{12}, \qquad (4.26)
\end{aligned}$$

with $\ddot{h}_{ij}$ determined by Eqs. (4.20), (4.21).

If this is not the case and $\ddot{h}_{23} = as_{12}c_{12}\sin(\Theta_{13}-\theta_{13})$ cannot be neglected, i.e. Θ_{13} is significantly larger than θ_{13}, then Θ_{12} in Eq. (4.24) comes to $\pi/2$ (0 with $V<0$, antineutrinos), see Fig. 4.2, and the *12* rotation in Eq. (4.23) does not effectively change the absolute values of elements in $\ddot{\mathcal{H}}$, but can only mix up their position in the matrix nullifying the 1-2 element, which is now negligible, at the same time.

Either way, the remaining 2-3 element disappears after another *23* rotation [14]

$$\dddot{\mathcal{H}} = U_{23}(\tilde{\theta}_{23})\mathcal{H}_m U_{23}(\tilde{\theta}_{23})^\dagger \qquad (4.27)$$

with an angle

$$\tan 2\tilde{\theta}_{23} = \frac{2\ddot{h}_{23}}{\ddot{h}_{33}-\ddot{h}_{22}} = \frac{a\sin 2\theta_{12}\sin(\Theta_{13}-\theta_{13})}{\frac{2EV}{\Delta m^2}\cos^2\Theta_{13} + \sin^2(\Theta_{13}-\theta_{13}) - a[c_{12}^2 - s_{12}^2\cos^2(\Theta_{13}-\theta_{13})]}, \qquad (4.28)$$

which produces additional corrections of the next order of a [14].

4.3.1 Effective mixing matrix and angles in matter

According to the diagonalization of $\mathcal{H}$ described above, the mixing matrix between flavor states $|\nu_\alpha\rangle$ and effective mass eigenstates in media $|N_i\rangle$ is approximately [14, 26]

$$\mathcal{U} \approx U_{23}(\theta_{23})I_\delta U_{13}(\Theta_{13})U_{12}(\Theta_{12})U_{23}(\tilde{\theta}_{23}), \qquad (4.29)$$

where the last *23* rotation is small comparing to the first three, or, the effective 23-mixing angle in matter $\approx \theta_{23}$. Notice that elements of mixing matrix $\mathcal{U}$ are, contrary to vacuum,

[2)] Notice again, oscillations depend on relative phases, that means differences of eigenvalues of the Hamiltonian, not on their absolute scales.

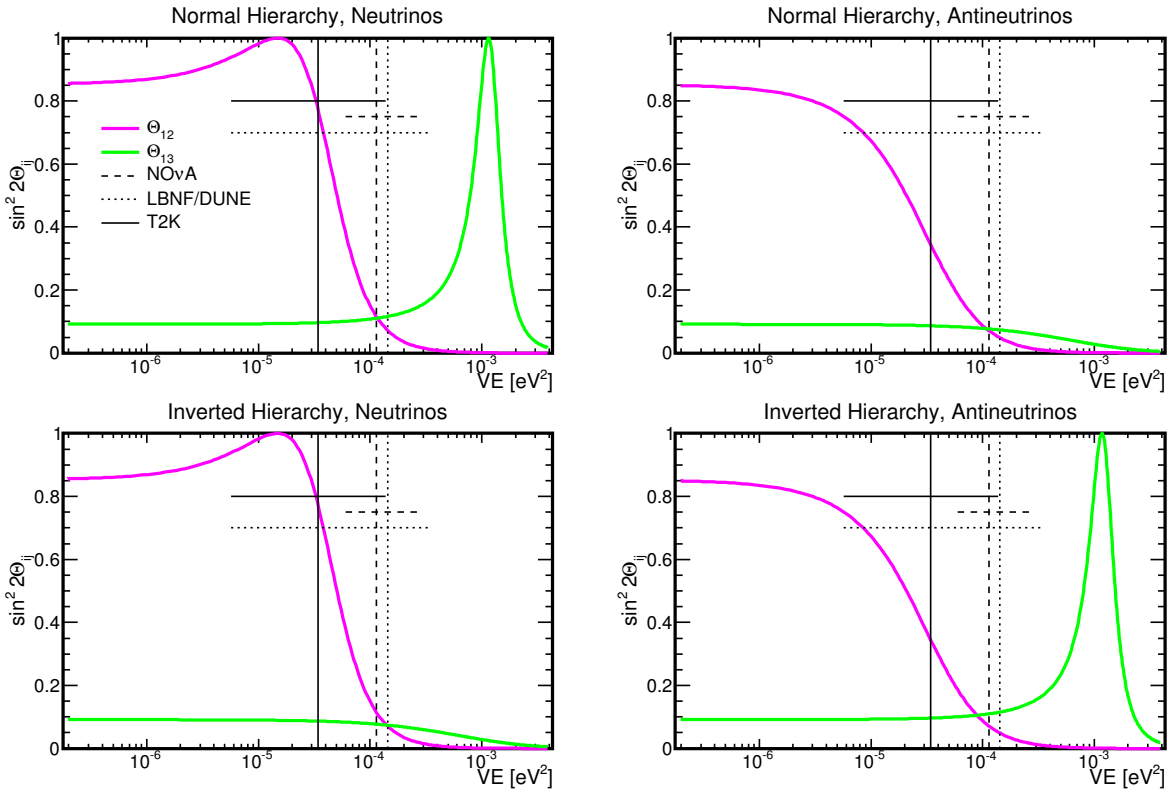

Figure 4.2: The dependence of effective matter mixing angles $\sin^2 2\Theta_{ij}$ on the product of potential and neutrino energy VE. Corresponding range of neutrino energy spectra (horizontal lines) and their peaks (vertical lines) for NOνA (dashed), LBNF/DUNE (dotted) and T2K (full) marked out. All parameters as in Table 2.1, $\theta_{23} = 45°$. **Left semi-plane:** For neutrinos. **Right semi-plane:** For antineutrinos. **Upper semi-plane:** For normal hierarchy. **Lower semi-plane:** For inverted hierarchy.

functions of energy E and in density varying profiles also functions of L ($\mathcal{U}$ differs with spatial variable).

In contrast to θ_{23}, angles Θ_{13} determined by Eq. (4.19)

$$\tan 2\Theta_{13} = \frac{\sin 2\theta_{13}}{\cos 2\theta_{13} - \frac{2EV}{\Delta m^2(1-as^2_{12})}} \tag{4.30}$$

and Θ_{12} from Eq. (4.24)

$$\tan 2\Theta_{12} = \frac{a \sin 2\theta_{12} \cos(\Theta_{13} - \theta_{13})}{a[c^2_{12} - s^2_{12}\cos^2(\Theta_{13} + \theta_{13})] - \sin^2(\Theta_{13} + \theta_{13}) - \frac{2EV}{\Delta m^2}\cos^2\Theta_{13}} \tag{4.31}$$

can be considerably distinct from their vacuum counterparts depending on the product VE. Fig. 4.2 shows $\sin^2 2\Theta_{12}$ and $\sin^2 2\Theta_{13}$ with respect to VE in case of neutrinos/antineutrinos and normal/inverted mass ordering. The 12-resonance occurs only for $VE > 0$ (neutrinos), since $\Delta m^2_{21} > 0$. Position of the 13-resonance is connected with the sign of Δm^2 and is not known yet.

4.3.2 Effective neutrino masses in matter

The effective eigenvalues are the diagonal elements of $\mathcal{H}_m$ obtained via last *23* rotation in Eq. (4.27) and they have been previously denoted (Eq. (4.10)) as $M_i^2/2E$ with effective masses of neutrinos M_i^2. The rotation over $\tilde{\theta}_{23}$ obviously does not affect 1-1 element of $\ddot{\mathcal{H}}$ in Eq. (4.23), hence from Eq. (4.25)

$$M_1^2 \approx \Delta m^2 \ddot{\ddot{h}}_{11} = \Delta m^2 \left(\ddot{h}_{11}\cos^2\Theta_{12} + \ddot{h}_{22}\sin^2\Theta_{12} - \ddot{h}_{12}\sin 2\Theta_{12} \right) \tag{4.32}$$

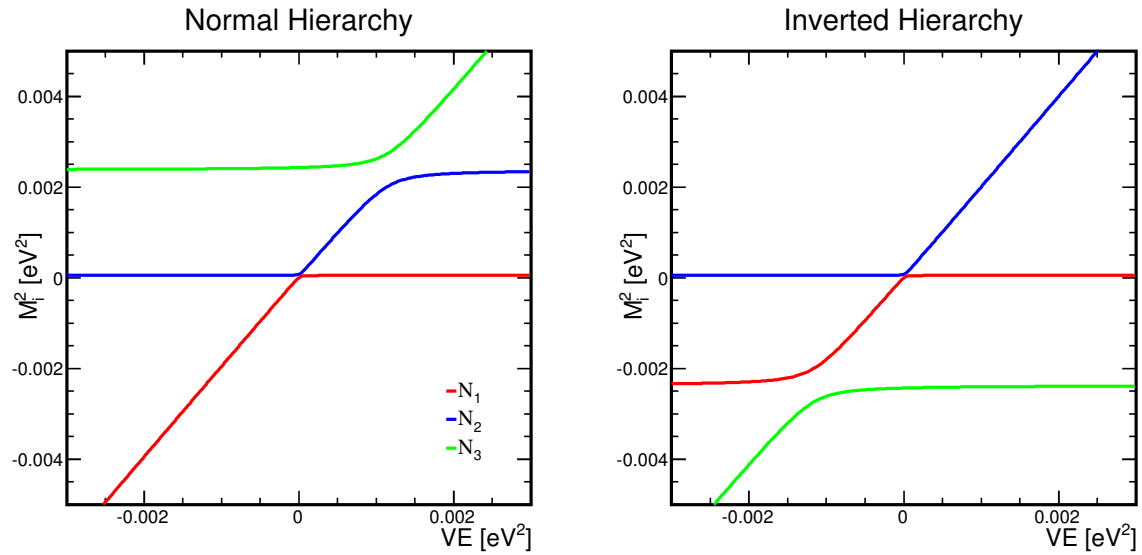

Figure 4.3: The energy level scheme. Effective eigenvalues M_i^2 of Hamiltonian in matter $\mathcal{H}$ as functions of VE. Note that for $VE \to 0$ Δm^2_{21} and Δm^2 are recovered. Oscillation parameters as in Table 2.1, $\theta_{23} = 45°$. **Left:** For normal hierarchy. **Right:** For inverted hierarchy. Denotation of the effective mass eigenstates (N_1, N_2, N_3) respects the standard convention, i.e. $M_1^2 < M_2^2 < M_3^2$ in case of normal hierarchy and $M_3^2 < M_1^2 < M_2^2$ in case of inverted hierarchy. $VE < 0$ reflects the antineutrino case.

with $\ddot{h}_{ij}$ from Eq. (4.20). Similarly 3-3 element is not affected by the last but one *12* rotation in Eq. (4.23), i.e. $\dddot{h}_{33} = \ddot{h}_{33}$, and consequently

$$M_2^2 \approx \Delta m^2 \left(\dddot{h}_{22} \cos^2 \tilde{\theta}_{23} + \ddot{h}_{33} \sin^2 \tilde{\theta}_{23} + \mathcal{O}(a^2) \right), \tag{4.33}$$

$$M_3^2 \approx \Delta m^2 \left(\dddot{h}_{22} \sin^2 \tilde{\theta}_{23} + \ddot{h}_{33} \cos^2 \tilde{\theta}_{23} + \mathcal{O}(a^2) \right), \tag{4.34}$$

where $\mathcal{O}(a^2)$ emerges from $\sin 2\tilde{\theta}_{23}$ and off-diagonal 2-3 element of $\dddot{\mathcal{H}}$. The values of M_i^2 as functions of VE are in Fig. 4.3. Because the absolute scale of neutrino masses has been unstrapped, M_i^2 do not represent actual masses and can be therefore negative. This has no physical aftermaths concerning e.g. imaginary square roots of M_i^2, since oscillation probabilities will depend on differences of M_i^2 only. Effective squared-mass splittings similar to Eq. (2.22) can be introduced:

$$\Delta M^2_{ij} = M_i^2 - M_j^2. \tag{4.35}$$

4.3.3 Resonance conditions and total flavor transitions

The positions of resonances (level crossings), which were already spoken of and can be seen in Figs. 4.2 and 4.3, are defined as a size of V for certain E, where the mixing in a given ij-plane is maximal, or $\sin^2 2\Theta_{ij} = 1, \Theta_{ij} = \pi/4$ [14]. This mechanism leads to possible total transitions between neutrino flavors and is called MSW effect, after Mikheev, Smirnov and Wolfenstein [1, 2, 14]. There are two resonances in the case of 3ν-model: the high 13-resonance and the low 12-resonance.

1. The high-resonance is associated with Δm^2 and θ_{13}. From Eq. (4.30) the mixing is maximal at

$$V_{13} = \cos 2\theta_{13}(1 - a s^2_{12}) \frac{\Delta m^2}{2E}. \tag{4.36}$$

2. The low-resonance is associated with Δm^2_{21} and θ_{12}. The simplest way to find its approximate location is to assume a 2ν-model [1, 7], or switch the rotations from Eq. (4.23) and Eq. (4.18) and neglect the small parameter s^2_{13}:

$$V_{12} \approx \cos 2\theta_{12} \frac{\Delta m^2_{21}}{2E}. \tag{4.37}$$

One could also use Eq. (4.24) and solve $\ddot{h}_{11} = \ddot{h}_{22}$. Hamiltonian elements were expressed only recursively with new effective rotation angles. But, according to Ref. [14] this will lead to

$$V_{12} \approx \cos 2\theta_{12} \frac{\Delta m^2_{21}}{2E} \frac{1}{c^2_{13}}, \tag{4.38}$$

which is also approximative and differs from the prior term by a factor $1/c^2_{13} \approx 2.5\%$.

Consider now, for simplicity, a 2ν-model (2 flavors α, β, 2 mass states $|\nu_1\rangle$, $|\nu_2\rangle$ and 2 matter mass states, see Refs. [1, 2]). The resonance condition (maximal mixing) means, that a flavor content of one effective mass eigenstate $|N_1\rangle$ is equal to $|N_2\rangle$, i.e. they contain the same amounts of $|\nu_\alpha\rangle$ and $|\nu_\beta\rangle$. Also, the effective squared-mass splitting ΔM^2_{ij} reaches its minimum at resonance. If the resonance is crossed adiabatically ($\mathrm{d}\Theta_{ij}(x)/\mathrm{d}x$ is small in comparison to ΔM^2_{ij} [1]), it can be understood as if the mass eigenstates swap the flavor contents with each other, so neutrino of flavor α becomes β and β becomes α. This is generally called an adiabatic flavor transition or total flavor transition, see Refs. [1, 2, 8]. It could be also explained in words of mass transition, when a mass eigenstate i becomes j and j becomes i[3)]. But, in this interpretation, transitions are not continuous, but a jump of magnitude ΔM^2_{ij} in M^2_i occur as one can convince themself in Fig. 4.3 (the blue and green lines would change their places, when $VE > V_{13}E$ and normal hierarchy, assuming only N_2 and N_3, for instance). However, in 3ν-model this keeps valid only for maximal 23-mixing, i.e. $\sin^2 2\theta_{23} = 1$. Otherwise, the parametrization in Eq. (2.8) leads to the same amount of $|\nu_e\rangle$ in $|N_1\rangle$ and $|N_2\rangle$ for $\sin^2 2\Theta_{12} = 1$ and that $|N_3\rangle$ is composed of 50% $|\nu_e\rangle$ and 50% mixture of $|\nu_\mu\rangle, |\nu_\tau\rangle$ while $\sin^2 2\Theta_{13} = 1$.

Reader can see in Figs. 4.2 and 4.3 that the oscillation parameters differ in case of neutrinos ($V > 0$) and antineutrinos (V can be effectively taken < 0, $\delta \to -\delta$), normal and inverted mass ordering. This is caused by inherent CP-assymetry of matter (there is a lot of electrons, but no positrons), which effectively increases the mass of ν_e, but lowers that of $\bar{\nu}_e$ [14, 30]. The positions (in neutrino/antineutrino sector) of both of the resonances depend on the sign of squared-mass splittings. Since the 12-resonance has been found by the solar experiments in oscillations of ν_e from thermonuclear reactions in the Sun, the 12-hierarchy $\Delta m^2_{21} > 0$ is resolved. To explore the second resonance, much higher energies of ν and/or matter densities are needed. The accelerator experiments with neutrinos at $\sim$ GeV and sufficient length of baselines in oscillation maxima and minima are very good candidates in this search. The expected neutrino spectra and their peaks of recent experiments T2K, NOνA [12] and future LBNF/DUNE [15] are marked out in Fig. 4.2.

4.4 Oscillation probabilities in matter with constant density

Oscillations in media with constant and isotropic density profile are the least complicated kind of oscillations to study while in matter. The potential V is then obviously also constant with respect to spatial variable L and hence the flavor composition (mixing angles) and eigenvalues of $\mathcal{H}$ do not change with L and are constant too. The oscillation probabilities have the same form as in vacuum in Eq. (2.21). To generalize it and get the matter probabilities is quite straightforward [14]

[3)] Formally this is just a rotational rearrangement of the flavor or mass eigenstates basis to keep the other one in the right order.

$$
\begin{aligned}
P(\nu_\alpha \to \nu_\beta; L, E) &= |\mathrm{Amp}(\nu_\alpha \to \nu_\beta; L, E)|^2 = \\
&= \left| \sum_{i=1}^{3} \mathcal{U}^*_{\alpha i} \mathcal{U}_{\beta i} \exp\left(-\mathrm{i}\frac{M_i^2}{2E} L\right) \right|^2 = \\
&= \sum_{i=1}^{3} \sum_{j=1}^{3} \mathcal{U}^*_{\alpha i} \mathcal{U}_{\alpha j} \mathcal{U}_{\beta i} \mathcal{U}^*_{\beta j} \exp\left(-\mathrm{i}\frac{\Delta M_{ij}^2}{2E} L\right), \qquad (4.39)
\end{aligned}
$$

where the elements of vacuum mixing matrix $U_{\alpha i}$ were traded for elements of effective matter mixing matrix $\mathcal{U}_{\alpha i}$ and vacuum squared masses m_i^2 for effective matter masses M_i^2. Notice again, that, unlike in vacuum, not only the argument of exp function is energy dependent. So are the elements of $\mathcal{U}$, thus the vacuum oscillatory pattern of neutrino flavor transition will be distorted.

For the needs of this text, it is not necessary to bring out additional solvable examples of neutrino propagation in matter like adiabatic conversions, small matter effects, propagation in multilayer medium, high energy neutrinos etc. Reader can consult Ref. [1, 14] to get more information on these phenomena.

5. Hierarchy determination, CP violation and $\nu_\mu \to \nu_e$ channel

This chapter examines the possibility of determining neutrino mass hierachy employing matter effects delineated in Chapter 4. Section 5.1 explains the importance of possible resonances in mass hierarchy resolution and introduces so-called "extrinsic" CP violation in neutrino oscillations, see also Refs. [1, 2, 5, 14, 30]. Section 5.2 presents the formula for ν_e appearance probability in ν_μ at atmospheric scales, often used in long-baseline neutrino experiments. Refs. [3, 14, 26, 27] can offer more details. Sections 5.3, 5.4 and 5.5 aim at the question of degenerate solutions of the mass hierarchy problem in $\nu_\mu \to \nu_e$ channel according to experimental uncertainties in CP phase δ, mixing angle θ_{13} and θ_{23}-octant respectively. Similar considerations are taken into account in experimental sensitivity studies such as in Refs. [15, 31, 32, 33].

5.1 Mass hierarchy determination using matter resonances

Suppose you are about to determine the mass hierachy of neutrino mass states. How would you do that? There is a simple way, that uses matter effects described in the last chapter. As it was mentioned and can be seen in Eqs. (4.36) and (4.37), the position of the resonance depends on Δm^2_{ij} including its sign, or

$$V_{ij} \gtrless 0 \Leftrightarrow \Delta m^2_{ij} \gtrless 0 \tag{5.1}$$

with V_{ij} being one of the resonance potentials. The VE resonance proximity influences the oscillations either of neutrinos ($V > 0$), or of antineutrinos ($V < 0$), not both of them at the same time. If a resonance takes place, corresponding mixing angle gets effectively larger up to $\pi/4$, where the mixing is maximal $\sin^2 2\Theta_{ij} = 1$, and with further density VE growth goes to $\pi/2$, see Fig. 4.2. If resonance does not take place (and is located in CP mirror sector), mixing angle gets effectively smaller going to 0. In appropriate channel of oscillations (e.g. $\nu_\alpha \to \nu_\alpha$ and $\nu_\alpha \to \nu_\beta$) this enlarges $P(\nu_\alpha \to \nu_\beta)$ and lowers $P(\nu_\alpha \to \nu_\alpha)$ comparing to vacuum while at resonance, but lowers $P(\nu_\alpha \to \nu_\beta)$ and enlarges $P(\nu_\alpha \to \nu_\alpha)$ while in sector without resonance. Notice, that the alternation of effective matter masses M^2_i, Fig. 4.3, do not affect this phenomenon, as their splittings ΔM^2_{ij} only change the L/E scale, where the oscillation minima/maxima lie, i.e. where the probability modification would be most significant.

For instance, ν_e disappearance at the solar scales (Eq. (2.28)) is governed by $\sin^2 2\theta_{12}$ (using Eq. (2.33)). Since a deficit of solar ν_e has been observed regarding SSM and oscillations [1, 2, 4, 10], the 12-resonance must be located in neutrino sector ($V_{12} > 0$) and the consequent 12-hierarchy $\Delta m^2_{21} > 0$. This is, of course, much simpler than reality, because solar neutrinos propagate through varying density profile (corresponding Θ_{12} is therefore spatial dependent, solar density profile covers values of V from high above the resonance $V \gg V_{12}$ to vacuum $V = 0$, neutrino crosses the resonance and total flavor transitions take place) from inside the Sun and then travel a vast distance in space vacuum towards the Earth (see Ref. [1] or [10] if interested). But, the main principle stay valid. Notice, that the conclusion would be identical even if it were antineutrinos, which are born in the Sun and detected in solar experiments. If so, there would be no resonance and Θ_{12} would get smaller than θ_{12} enhancing thus the total $\bar{\nu}_e$ flux. Ergo, again Δm^2_{21} has to be positive.

By the same token, the 13(23)-hierarchy could be resolved. The promising channel would be $\nu_\mu \to \nu_e$ transitions, since they are controlled by the combination $\sin^2 2\theta_{13} \sin^2 \theta_{23}$

from Eq. (2.31) at the atmospheric scales (Eq. (2.27)). To observe effective amplification or attenuation of oscillation probabilities, much greater densities or neutrino energies (VE) are needed than in solar case. Also, with VE in the resonance area, typical oscillation length in Eq. (2.25) gets longer as M_1^2 (IH) or M_2^2 (NH) goes to M_3^2. Provided terrestrial ambience (Earth's matter density and distances), high energy neutrino beams ($\sim$ GeV) with long oscillation baselines ($\sim 100 - 1000$ km) can offer such conditions. Although, one can see in Fig. 4.2, that recent experiments do not reach the resonance, only slight increase/decrease in Θ_{13}. Unfortunately, these relatively small matter effects can be misidentified with measured experimental uncertainties of some of the oscillation parameters, usually called δ-, θ_{13}- and θ_{23} octant-degeneracy [31, 32, 33]. They will be described in the very next paragraphs.

5.1.1 Matter induced extrinsic CP assymetry in neutrino oscillations

As already stated, the distinguish behavior of neutrino and antineutrino oscillations in media is caused by the inner composition of matter (no positrons) and is known as "extrinsic" or fake CP violation [30]. It is completely dissimilar to CP violation described in Section 2.3, which is ruled by the value of the CP phase δ. T mirror probabilities in matter cannot be generally expressed in terms of Eq. (2.35), moreover, symmetric density profiles do not cause any fake T violation at all, affecting $P(\nu_\mu \to \nu_e)$ and $P(\nu_e \to \nu_\mu)$ in the same manner [16]. Even in assymetric Earth profiles matter induced T violation is expected to be very small, if any.

5.2 $\nu_\mu \to \nu_e$ appearance probability in matter

Besides Eq. (4.39), which could be instantly used to get ν_e appearance probabilities in ν_μ beam with all effective matter parameters retrieved during the diagonalization of matter Hamiltonian in Section 4.3, the $P(\nu_\mu \to \nu_e)$ can be expressed explicitly with respect to vacuum parameters up to the second order in θ_{13} and $a = \Delta m^2_{21}/\Delta m^2$, see Refs. [3, 26],

$$\begin{aligned} P(\nu_\mu \to \nu_e) &= \sin^2 2\theta_{13} \sin^2\theta_{23} \frac{\sin^2\left[\left(\frac{V}{2} - \frac{\Delta m^2}{4E}\right) L\right]}{\left(\frac{2EV}{\Delta m^2} - 1\right)^2} + \\ &+ a \cos\theta_{13} \sin 2\theta_{13} \sin 2\theta_{12} \sin 2\theta_{23} \cos\left(\frac{\Delta m^2}{4E} L - \delta\right) \frac{\sin\left(\frac{V}{2} L\right)}{\frac{2EV}{\Delta m^2}} \frac{\sin\left[\left(\frac{V}{2} - \frac{\Delta m^2}{4E}\right) L\right]}{1 - \frac{2EV}{\Delta m^2}} \\ &+ a^2 \sin^2 2\theta_{12} \cos^2\theta_{13} \cos^2\theta_{23} \frac{\sin^2\frac{V}{2} L}{\left(\frac{2EV}{\Delta m^2}\right)^2} \end{aligned} \tag{5.2}$$

with V from Eq. (4.5) and formal exchange $V \to -V$, $\delta \to -\delta$ in the case of antineutrinos. According to the recent status of measured parameters (Table 2.1), the first term $\propto \sin^2 2\theta_{13} \approx 0.09$ is much greater than the second one $\propto a \sin 2\theta_{13} \approx 0.009$ and the last term $\propto a^2 \approx 0.0009$ is completely negligible. Results obtained via this explicit formula or stepwise diagonalization of $\mathcal{H}_f$ from Eq. (4.12) are in general congruence at atmospheric scales and applicable for the purposes of the long-baseline experiments [14, 26, 27].

Figs. 5.1, 5.2 and 5.3 show the dependence of $P(\nu_\mu \to \nu_e)$ on energy E for three experimental layouts: NOνA (810 km), T2K (295 km) and future LBNF/DUNE (1300 km) respectively, with uniform density parameter $\frac{G_F N_e}{\sqrt{2}} = \frac{1}{3500 \text{ km}}$ [22] and maximal 23-mixing $\theta_{23} = 45°$. Despite the global fit from Ref. [3] in Table 2.1 favors $\delta \in [\pi, 2\pi]$, the full $[0, 2\pi]$ interval is being probed (so will be later on in the text). Variation of δ leads to the dotted regions in the plots.

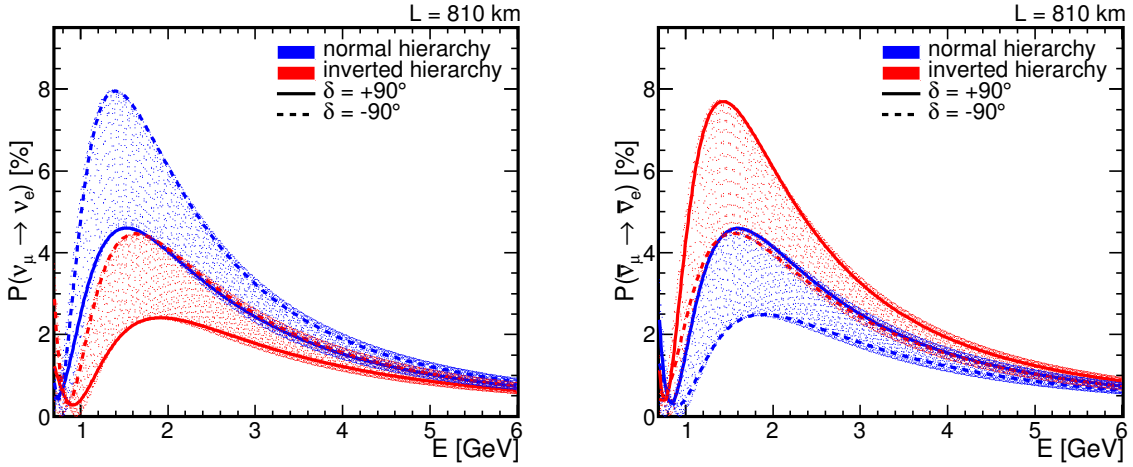

Figure 5.1: Appearance probability of ν_e for initial ν_μ in matter as a function of energy E at NOνA: $L = 810$ km, $\frac{G_F N_e}{\sqrt{2}} = \frac{1}{3500\ \text{km}}$, $\theta_{23} = 45°$, $\delta \in [0; 2\pi]$, other parameters from Table 2.1. **Left:** For neutrinos $\nu_\mu \to \nu_e$. **Right:** For antineutrinos $\bar{\nu}_\mu \to \bar{\nu}_e$.

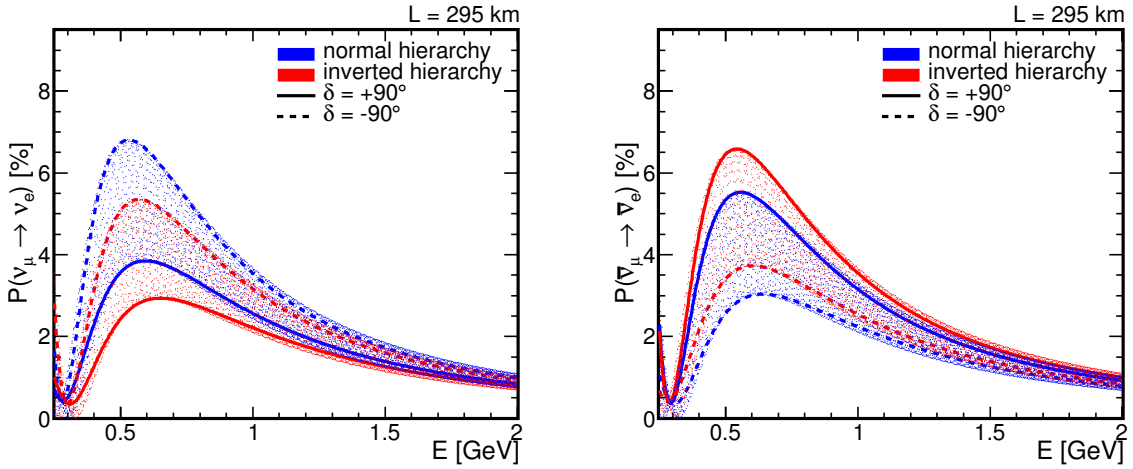

Figure 5.2: Appearance probability of ν_e for initial ν_μ in matter as a function of energy E at T2K: $L = 295$ km, $\frac{G_F N_e}{\sqrt{2}} = \frac{1}{3500\ \text{km}}$, $\theta_{23} = 45°$, $\delta \in [0; 2\pi]$, other parameters from Table 2.1. **Left:** For neutrinos $\nu_\mu \to \nu_e$. **Right:** For antineutrinos $\bar{\nu}_\mu \to \bar{\nu}_e$.

5.3 Intrinsic CP violation and δ degeneracy

The second term in Eq. (5.2) or I_δ in Eq. (4.29) carrying δ are responsible for possible CP violation. This one is called "intrinsic" CP violation as it is caused by the nature of neutrino oscillations itself and not by the presence of media. The magnitude of CPV effects depends on the size of δ, being maximal at $\delta = \pi$ and minimal at $\delta = 0, 2\pi$. Hence, intrinsic CPV is different from matter induced CPV, which relies on the formal sign and value of the potential V. Working together they can amplify their impact on the transition probabilities making them larger/smaller or go against each other and cancel mutually.

The possible arrangements allowed by the odds - normal hierarchy (NH), inverted hierarchy (IH), upper hyper-plane (UHP) $\delta \in [0°, 180°]$, lower hyper-plane (LHP) $\delta \in [-180°, 0°]$ - are:

1. **NH-UHP:** ν - the first term in Eq. (5.2) is increased (effective enhancement of θ_{13} in matter to eff. Θ_{13}) and this is compensated by the second term, which lowers the overall $P(\nu_\mu \to \nu_e)$ due to the value of δ; $\bar{\nu}$ - the whole consideration is re-

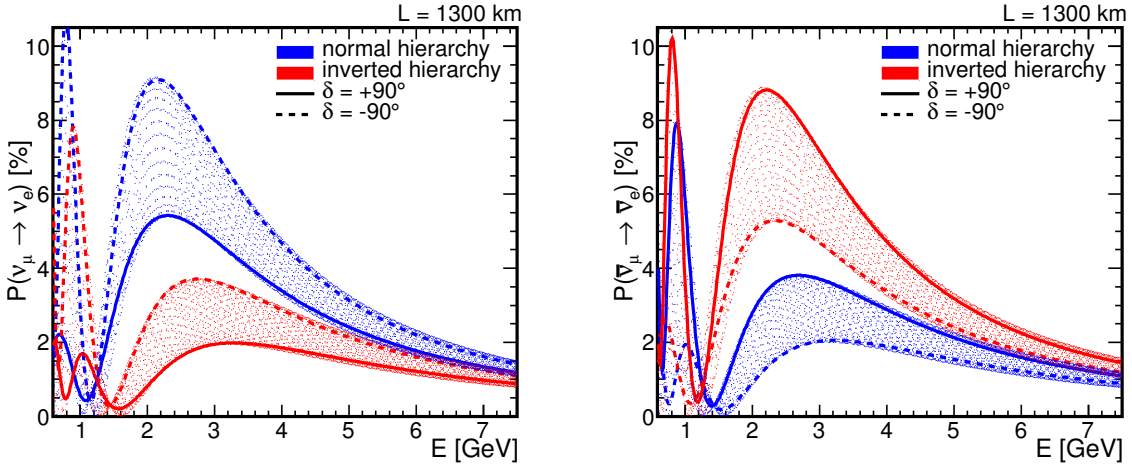

Figure 5.3: Appearance probability of ν_e for initial ν_μ in matter as a function of energy E at LBNF/DUNE: $L = 1300$ km, $\frac{G_F N_e}{\sqrt{2}} = \frac{1}{3500 \text{ km}}$, $\theta_{23} = 45°$, $\delta \in [0; 2\pi]$, other parameters from Table 2.1. **Left:** For neutrinos $\nu_\mu \to \nu_e$. **Right:** For antineutrinos $\bar{\nu}_\mu \to \bar{\nu}_e$.

versed: the first term in $P(\bar{\nu}_\mu \to \bar{\nu}_e)$ would be lowered, but the second one is enlarged. Oscillations mimic no CPV (intrinsic and extrinsic) at all in this case (as if they were in vacuum with $\delta = 0$).

2. **NH-LHP:** ν - θ_{13} is effectively larger, intrinsic CPV effects enlarges $P(\nu_\mu \to \nu_e)$; $\bar{\nu}$ - θ_{13} gets effectively smaller, intrinsic CPV effects lowers $P(\bar{\nu}_\mu \to \bar{\nu}_e)$. Oscillations suffer from maximal CPV and are significantly different from vacuum case.
3. **IH-UHP:** ν - θ_{13} is effectively smaller, intrinsic CPV effects lowers $P(\nu_\mu \to \nu_e)$; $\bar{\nu}$ - θ_{13} is effectively larger, intrinsic CPV effects enlarges $P(\bar{\nu}_\mu \to \bar{\nu}_e)$. Oscillations suffer from maximal CPV and are significantly different from vacuum case.
4. **IH-LHP:** ν - θ_{13} is effectively smaller, but intrinsic CPV effects enlarges $P(\nu_\mu \to \nu_e)$; $\bar{\nu}$ - θ_{13} is effectively larger, but intrinsic CPV effects lowers $P(\bar{\nu}_\mu \to \bar{\nu}_e)$. Oscillations mimic no CPV (intrinsic and extrinsic) at all in this case.

In order to determine the mass hierarchy $P(\nu_\mu \to \nu_e)$ and $P(\bar{\nu}_\mu \to \bar{\nu}_e)$ are measured and compared with expected values in cases of NH and IH. In Figs. 5.1 and 5.2 one can recognize areas, where the points belonging to NH can be misidentified with those from IH. This happens when unfavorable conditions NH-UHP or IH-LHP take place and would be usually designated as a region of δ-degeneracy. LBNF/DUNE sits (will sit) ahead of the second oscillation maximum (1300 km), where the degeneracy regions separates from one another, see Fig. 5.3.

Fig. 5.4 is a typical biprobability plot for NOνA: $L = 810$ km and $E = 2.0$ GeV. Certain oscillation parameters and L, E pinpoint two ellipses in such a plot for normal and for inverted hierachy along which the CP phase δ varies. All the points near the $P(\nu_\mu \to \nu_e) = P(\bar{\nu}_\mu \to \bar{\nu}_e)$ axis are unfavorable for the intents of mass hierarchy determination and correspond to the regions of δ-degeneracy NH-UHP, IH-LHP. In case of NH-LHP and IH-UHP the mass hierarchy determination is possible at NOνA, in case of NH-UHP or IH-LHP NOνA has no hierarchy sensitivity. The figure also illustrates 1σ (dashed) and 2σ (full) intervals for measured probabilities with 3 years ν and 3 years $\bar{\nu}$ run. The same kind of biprobability plots for T2K and LBNF/DUNE at their peaks of expected $\nu_e/\bar{\nu}_e$ spectrum are in Fig. 5.5.

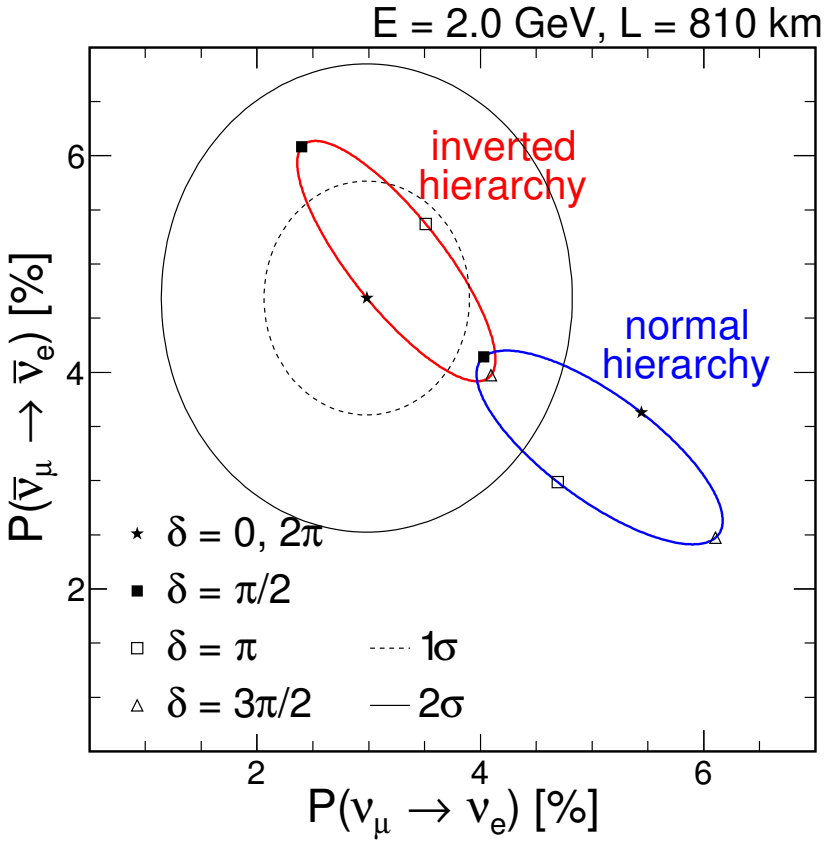

Figure 5.4: The biprobability plot at NOνA: $L = 810$ km, $E = 2.0$ GeV, $\frac{G_F N_e}{\sqrt{2}} = \frac{1}{3500\ \text{km}}$, $\theta_{23} = 45°$, other parameters as in Table 2.1. Estimated 1σ (dashed) and 2σ (full) contours for $\delta = 0$ (starred point) in case of inverted hierarchy marked out.

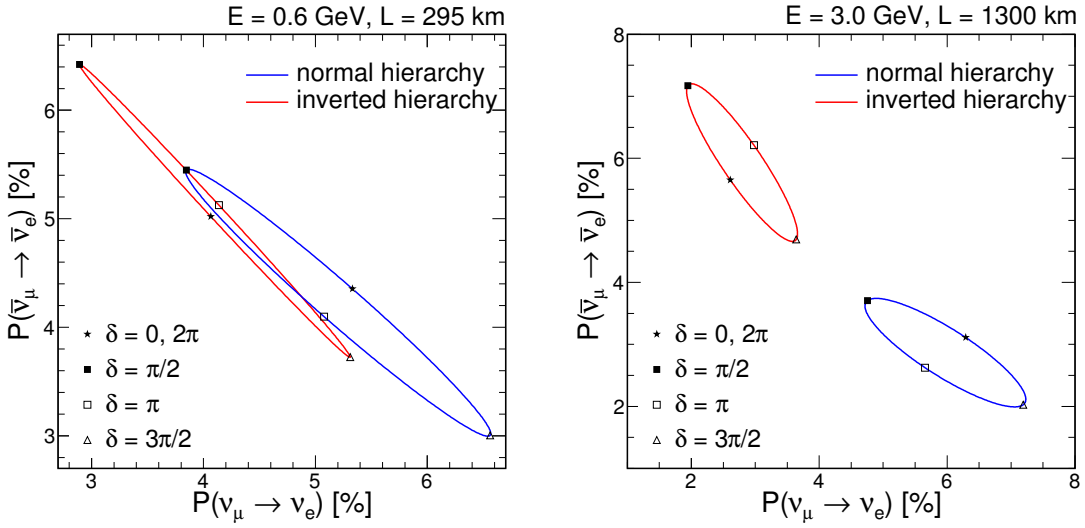

Figure 5.5: Biprobability plots at T2K and LBNF/DUNE at the peaks (expected in the case of LBNF/DUNE, see [15]) of their ν_e spectra. **Left:** T2K: $L = 295$ km, $E = 0.6$ GeV, $\frac{G_F N_e}{\sqrt{2}} = \frac{1}{3500\ \text{km}}$, $\theta_{23} = 45°$. **Right:** LBNF/DUNE: $L = 1300$ km, $E = 3.0$ GeV, $\frac{G_F N_e}{\sqrt{2}} = \frac{1}{3500\ \text{km}}$, $\theta_{23} = 45°$. Other parameters from Table 2.1.

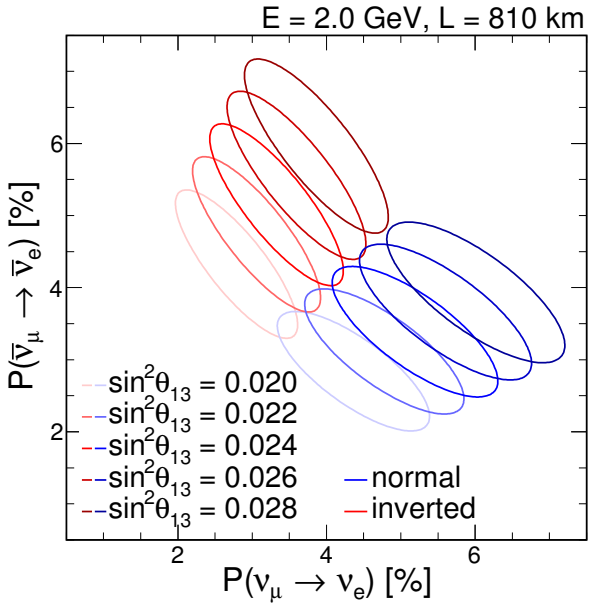

Figure 5.6: The biprobability plot showing the dependence on the size of θ_{13} at NOνA: $L = 810$ km, $E = 2.0$ GeV, $\frac{G_F N_e}{\sqrt{2}} = \frac{1}{3500\ \text{km}}$, $\theta_{23} = 45°$. Other parameters as in Table 2.1.

5.4 θ_{13} degeneracy

Another considerable degeneracy in mass hierarchy determination that can limit the experimental sensitivity is the θ_{13} uncertainity. For example, matter enhancement (decrease) of vacuum θ_{13} to effective Θ_{13} can be cancelled by choosing lower (higher) initial value of θ_{13} within the interval allowed by the experimental fits. But, the crucial observation is, that a combination of ν and $\bar{\nu}$ data on oscillation probabilities do not sustain this disadvantage [31]. As long as $P(\nu_\mu \to \nu_e, \theta_{13}, \text{NH}) \approx P(\nu_\mu \to \nu_e, \hat{\theta}_{13}, \text{IH})$, where $\theta_{13} \neq \hat{\theta}_{13}$, $P(\bar{\nu}_\mu \to \bar{\nu}_e, \theta_{13}, \text{NH})$ would be significantly smaller than $P(\bar{\nu}_\mu \to \bar{\nu}_e, \hat{\theta}_{13}, \text{IH})$. Thus, it is vital to measure in both ν and $\bar{\nu}$ modes to resolve the θ_{13}-degeneracy and the mass hierarchy problem. Fig. 5.6 shows, how the position of the ellipses in the biprobability plot changes with θ_{13}.

5.5 Octant θ_{23} degeneracy

MINOS experiment [18] has measured a no maximal mixing in 23-sector $\sin^2 2\theta_{23} < 1$. This means there could be two degenerate solutions in lower octant (LO) $\sin^2\theta_{23} < 0.5$ and in higher octant (HO) $\sin^2\theta_{23} > 0.5$. Eq. (2.41) gives 90% C.L. interval for $\sin^2\theta_{23} \in [0.36, 0.65]$ (it is convenient to take a symmetric interval $[0.35, 0.65]$). With combinations from Section 5.3 this results in eight possible situations: **NH-UHP-HO**, **NH-UHP-LO**, **NH-LHP-HO**, **NH-LHP-LO**, **IH-UHP-HO**, **IH-UHP-LO**, **IH-LHP-HO**, **IH-LHP-HO**. Generally, θ_{23} from higher octant enhances the overall transition probability in Eq. (5.2), while θ_{23} from lower octant suppresses it in comparison to $\theta_{23} = 45°$. As a consequence, $P(\nu_\mu \to \nu_e$, NH-x-LO$) \approx P(\nu_\mu \to \nu_e$, IH-x-HO$)$ could be a degenerate solution of the mass hierarchy problem. However, similarly to previous section, this can be sorted out by additional information from $\bar{\nu}_\mu \to \bar{\nu}_e$ oscillations, since the degeneracy would not be present in antineutrinos oscillations. On the other hand, NH-LHP-HO and IH-UHP-LO cases could have a good hierarchy sensitivity even with pure ν data (provided no θ_{13}-degeneracy).

Moreover, Fig. 5.7 shows, that with θ_{23} being from HO, ellipses in the biprobability plot do not intersect each other any more and leave the δ-degeneracy region. Hence, with growing θ_{23} the mass hierarchy determination would be much easier. As an illustration, one can see

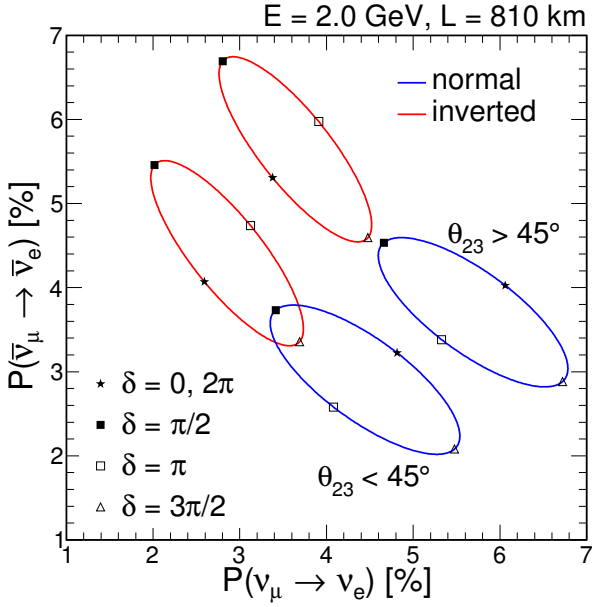

Figure 5.7: The biprobability plot showing the dependence on two possible scenarios $\theta_{23} > 45°$ and $< 45°$ at NOνA: $L = 810$ km, $E = 2.0$ GeV, $\frac{G_F N_e}{\sqrt{2}} = \frac{1}{3500 \text{ km}}$. Parameters as in Table 2.1.

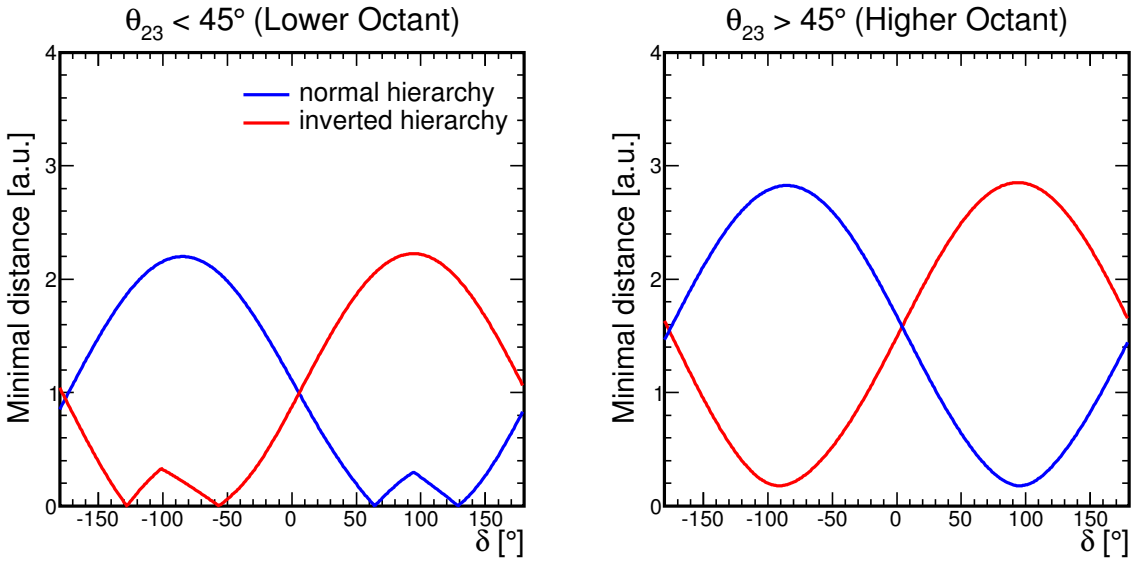

Figure 5.8: Dependence of the minimal distance of a point in a biprobability plot from points of vying hierarchy hypothesis on the true value of δ in units corresponding to % in the biprobability plots for NOνA: $L = 810$ km, $E = 2.0$ GeV, $\frac{G_F N_e}{\sqrt{2}} = \frac{1}{3500 \text{ km}}$. Scale of the "Minimal distance" axis correlates to the resolution given in % at which an experiment detects the appearance probability of ν_e and $\bar{\nu}_e$ and thus determines its ability to distinguish between points of opposite hierarchies for particular δ. **Left:** $\sin^2\theta_{23} = 0.44$ (NH), 0.46 (IH). **Right:** $\sin^2\theta_{23} = 0.56$ (NH), 0.54 (IH).

in Fig. 5.8 the minimal distance of a point on an ellipse from the points of counter-hypothesis (opposite hierarchy) as a function of δ at NOνA. The scale on the "minimal distance" axis is chosen to correlate with an experimental resolution at which an experiment can possibly measure the combined ν_e, $\bar{\nu}_e$ appearance probability, i.e. at which it can fix the position of a biprobability point in the $P(\nu_\mu \to \nu_e)$ vs. $P(\bar{\nu}_\mu \to \bar{\nu}_e)$ plane.

At last, and shall not be left out, $\nu + \bar{\nu}$ data has a relatively strong ability to resolve the question of θ_{23} octant itself specifying thus whether $\theta_{23} >$ or $< 45°$.

5.6 Summary of possibly realized scenarios

In conclusion, there are eight possible scenarios of oscillation parameters, which can be divided into two groups of favorable and unfavorable situations depending on the size of δ [31]. The unfavorable (hierarchy cannot be determined by recently active long-baseline experiments and will be more difficult even with future LBNF/DUNE or others) ones are:

1. **NH-UHP-LO** or **-HO**,
2. **IH-LHP-LO** or **-LO**.

The favorable (hierarchy can be determined by recently active long-baseline experiments at ca 2σ and with future improvement far over 5σ using LBNF/DUNE or others) ones are:

1. **NH-LHP-HO:** could be perchance resolved from ν data only.
2. **NH-LHP-LO:** could be perchance resolved from $\bar{\nu}$ data only.
3. **IH-UHP-HO:** could be perchance resolved from $\bar{\nu}$ data only.
4. **IH-UHP-LO:** could be perchance resolved from ν data only.

6. GLoBES

Chapter 6 introduces the simulation software GLoBES and its utilization in long-baseline experiments. Section 6.1 presents a brief note on the concept of GLoBES, much more to be seen in Refs. [34, 35, 36]. The basics of obtaining high-level information on experiment are in Section 6.2 and more tangibly in Refs. [34, 36]. The last Section 6.3 gives elementary comprehension of results retrieved by GLoBES necessary for further interpretation, see Refs. [34, 35, 36] and for statistics Refs. [37, 38, 39, 40].

6.1 Introduction and concept of GLoBES

GLoBES (General Long Baseline Experiment Simulator) [34, 35] is a software tool to simulate and analyze neutrino oscillation short- and long-baseline experiments in a complete 3ν-model. It allows to define an experiment at an abstract level with AEDL (Abstract Experiment Definition Language) specifying its parameters, i.e. baseline, fiducial mass, duration, energy resolution, neutrino energy window, neutrino flux power, density profile, energy dependent efficiencies and interpolation technique, channel definitions and rules (which dis/appearance channels of neutrino oscillations are measured). GLoBES simulates a stationary point source of neutrinos and, unfortunately, geometrical effects of a source distribution, such as in the Sun or the atmosphere, are not described. Also, sources with a physically significant time dependence (supernovae), cannot be studied [34]. In the systematics, energy normalization and calibration errors can be simulated. With GLoBES version 3.0 or higher almost all features can be user defined in order to provide more variability and adaptibility [36].

Typical input needed by a GLoBES script is a set of an experiment definition and detector properties, neutrino cross sections and oscillation parameters. The output will be energy binned event rates observed. Following analysis consists of finding the possible oscillation parameters (θ_{ij}, Δm^2_{ij}, δ) that could be in a good agreement with the data. This procedure allows to locate the degenerate solutions of particular neutrino oscillation problems and to estimate the experiment sensitivity to its resolution. The main advantage of GLoBES is handling multiple experiments at once, hence, combined sensitivities and global fits can be investigated.

Besides that, GLoBES offers also low-level information, e.g. oscillation probabilities, concrete event rates, fluxes, etc.

6.2 High-level experimental information with GLoBES

Given a vector of oscillation parameters, i.e. mixing angles, mass splittings, CP phase and a matter density profile and an experiment definition (all as *true values*), GLoBES simulates a vector of event rates, associated to each oscillation channel and rule, observed in a detector $\mathbf{n} \equiv (n_1, \ldots, n_N)$ [34] arranged in an energy histogram

$$\textit{true values of osc. parameters} \xrightarrow{\text{simulation}} \textit{observed event rates } (\boldsymbol{n}). \tag{6.1}$$

Poisson distribution of n_i in every bin is assumed [34]. To test a certain hypothesis of *test values* $(\boldsymbol{\lambda}, \mathbf{a})$ expected rates $\boldsymbol{\nu} \equiv (\nu_1, \ldots, \nu_N)$ are computed

$$\textit{estimated test values } (\boldsymbol{\lambda}, \mathbf{a}) \longrightarrow \textit{expected event rates } (\boldsymbol{\nu}) \tag{6.2}$$

and the value of $\chi^2(\boldsymbol{\lambda}, \mathbf{a})$ (explained in the very next section) is found [36]

$$\chi^2(\boldsymbol{\lambda}, \mathbf{a}) = 2 \sum_{\text{exps}} \sum_{\text{rules}} \sum_{\text{bins}} \left[\nu_i(\boldsymbol{\lambda}, \mathbf{a}) - n_i + n_i \ln \frac{n_i}{\nu_i(\boldsymbol{\lambda}, \mathbf{a})} \right] + \chi^2_{\text{prior}}(\boldsymbol{\lambda}) + \chi^2_{\text{pull}}(\mathbf{a}), \tag{6.3}$$

where the vectors $\boldsymbol{\lambda}, \mathbf{a}$ contain oscillation parameters and systematical biases respectively. $\chi^2_{\text{prior}}(\boldsymbol{\lambda})$ represents the treatment of previously determined parameters as Gaussian priors, $\chi^2_{\text{pull}}(\mathbf{a})$ implements external input on $\mathbf{a}$ with pull method [34, 36]. The sum is over all experiments, their rules and energy bins active in analysis.

GLoBES provides several built-in χ^2 functions to support different systematics, parameter correlations etc. A number of minimization procedures can be used including χ^2 projections in oscillation parameter space. It allows also for arbitrary, user-defined χ^2 functions and projections [34, 35, 36].

6.3 Remarks on simulation analysis

The value of $\chi^2(\boldsymbol{\lambda}, \mathbf{a})$ computed by GLoBES is a measure of how well the observed event rates $\mathbf{n}$ would be described by the parameters $\boldsymbol{\lambda}, \mathbf{a}$. One can see, neglecting systematics, that $\chi^2(\boldsymbol{\lambda}) = 0$ with $\boldsymbol{\lambda} = \textit{true values}$. To test a hypothesized value of parameters profile likelihood ratio is commonly employed, see Refs. [37, 38]. In the next paragraphs $\hat{\vartheta}$ denotes the maximum likelihood estimator of ϑ.

6.3.1 Poissonian data set

Consider a histogram of data $\mathbf{n} \equiv (n_i, \ldots, n_N)$ with N bins, where n_i are independent and Poisson distributed. The joint probability for $\mathbf{n}$ is

$$P(\mathbf{n}; \boldsymbol{\nu}) = \prod_{i=1}^{N} \frac{\nu_i^{n_i}}{n_i!} \exp(-\nu_i). \tag{6.4}$$

Regarding each mean value ν_i as adjustable, the maximum likelihood estimators of them would be $\hat{\nu}_i = n_i$ [37]. Suppose the tested hypothesis $\boldsymbol{\nu}$ can be determined through M parameters $\hat{\boldsymbol{\vartheta}} \equiv (\hat{\vartheta}_1, \ldots, \hat{\vartheta}_M)$. Using log-likelihood ratio, it is convenient to define a statistic

$$t_{\boldsymbol{\nu}} = -2 \ln \frac{L(\boldsymbol{\nu}(\hat{\boldsymbol{\vartheta}}))}{L(\hat{\boldsymbol{\nu}})} = 2 \sum_{i=1}^{N} \left[\nu_i(\hat{\boldsymbol{\vartheta}}) - n_i + n_i \ln \frac{n_i}{\nu_i(\hat{\boldsymbol{\vartheta}})} \right], \tag{6.5}$$

where $L(\cdot)$ is the likelihood function of Poisson distribution from Eq. (6.4) and $\hat{\boldsymbol{\nu}} = \mathbf{n}$.

From the Wilks' theorem, $t_{\boldsymbol{\nu}}$ in Eq. (6.5) follows asymptotically $\boldsymbol{\chi}^2_{(N-M)}$ distribution with $(N - M)$ degrees of freedom [37, 38]. In a model with normalized histograms $(N - 1)$ free parameters are in effect, since the total number of event rates, or the histogram area is fixed. Hence, there are $(N - N + 1) = 1$ degree of freedom.

The basic problem of maximizing the likelihood function in order to find $\hat{\boldsymbol{\vartheta}}$ is equivalent to finding a minimum of a quantity

$$\chi^2(\boldsymbol{\vartheta}) = 2 \sum_{i=1}^{N} \left[\nu_i(\boldsymbol{\vartheta}) - n_i + n_i \ln \frac{n_i}{\nu_i(\boldsymbol{\vartheta})} \right], \qquad \Delta\chi^2 = \min_{\boldsymbol{\vartheta}} \chi^2(\boldsymbol{\vartheta}) \tag{6.6}$$

with respect to $\boldsymbol{\vartheta}$ and the same estimators $\hat{\boldsymbol{\vartheta}}$ will result [37]. As an added bonus, the value of $\chi^2(\boldsymbol{\vartheta})$ can be directly used to test the goodness of fit and, if the Wilks' theorem is satisfied, its sampling distribution is $\boldsymbol{\chi}^2_{(N-M)}$ ($\boldsymbol{\chi}^2_{(1)}$ in a histogram model).

7. Study of mass hierarchy determination at NOνA

Chapter 7 revisits the study done in Ref. [31] probing the advantage of an early antineutrino run of NOνA. Section 7.1 explains the intents and motivation to study expected sensitivity to mass hierarchy at NOνA. Details of simulations done by GLoBES are listed in Section 7.2. Achieved results and their discussion can be found in Section 7.3.

7.1 Object, intents and motivation

As was explained in Chapter 5, the way to resolve the mass hierarchy is to measure $P(\nu_\mu \rightarrow \nu_e)$, $P(\bar{\nu}_\mu \rightarrow \bar{\nu}_e)$ or both, and it strongly depends on the precise values of θ_{13}, θ_{23} and, mainly, CP phase δ, whether this will lead to a final answer or degenerate solutions only (e.g. statement like "the hierarchy is either normal and $\delta \in [0, 180°]$, or inverted and $\delta \in [-180°, 0]$"). Recently, only NOνA and T2K search for ν_e appearance in ν_μ beams (also MINOS, see Ref. [18]), LBNF/DUNE is planned as a next future long-baseline experiment to start in 2020 or later [15]. T2K began its $\bar{\nu}$ period this year (2015) after 5 years of ν data taking, see Ref. [19]. NOνA is designed to run for 3 years in ν mode and 3 years in $\bar{\nu}$ [22]. There have been a number of studies of expected sensitivities to the mass hierarchy problem for both experiments and their combined analysis or with other types of experiments, e.g. atmospheric, see the proposals Refs. [20, 41] and Refs. [12, 32, 33, 42, 43, 44, 45, etc.]. All lead to similar conclusions, that NOνA alone can reject the wrong hierarchy hypothesis for ca 45% (NH-LHP, IH-UHP) of the possible δ interval $[0, 2\pi]$ at 90% C.L. with a slight improvement including T2K data (T2K alone has practically no hierarchy sensitivity [33, 45]).

As also already discussed, it is important to measure both ν and $\bar{\nu}$ oscillations to withdraw the imminent parameter degeneracies in θ_{13} and θ_{32}, to which pure ν data is subjected, whereas $\nu + \bar{\nu}$ data is not. The object of the following sections is to show, that considerable results upon the question of the mass hierarchy can be achieved sooner than scheduled, after 3 years of NOνA running (instead of 6), provided an earlier switch to antineutrino mode. In order to do so, GLoBES was used to simulate NOνA experiment and the expected sensitivity to the mass ordering was computed.

7.2 Simulation details

GLoBES 3.0.11 and NOνA experiment definition in 0709-nova.glb file[1)] with slight changes (close details in Table 7.1) were used in simulations, neutrino cross sections were taken from Ref. [46].

Six scenarios of true values of oscillation parameters (imagined as representatives being realized in nature) were considered (compare Table 2.1):

1. NH, $\sin^2\theta_{23} = 0.5$, $\sin^2\theta_{13} = 0.023$, $\delta \in [-180°, 180°]$ (Fig. 7.1),
2. NH-HO, $\sin^2\theta_{23} = 0.56$, $\sin^2\theta_{13} = 0.023$, $\delta \in [-180°, 180°]$ (Fig. 7.2),
3. NH-LO, $\sin^2\theta_{23} = 0.44$, $\sin^2\theta_{13} = 0.023$, $\delta \in [-180°, 180°]$ (Fig. 7.3),
4. IH, $\sin^2\theta_{23} = 0.5$, $\sin^2\theta_{13} = 0.024$, $\delta \in [-180°, 180°]$ (Fig. 7.1),
5. IH-HO, $\sin^2\theta_{23} = 0.54$, $\sin^2\theta_{13} = 0.024$, $\delta \in [-180°, 180°]$ (Fig. 7.2),
6. IH-LO, $\sin^2\theta_{23} = 0.46$, $\sin^2\theta_{13} = 0.024$, $\delta \in [-180°, 180°]$ (Fig. 7.3)

with $|\Delta m^2| = 2.4 \times 10^{-3}$ eV^2 and solar parameters $\sin^2\theta_{12} = 0.31$, $\Delta m^2_{21} = 7.5 \times 10^{-5}$ eV^2. For each of these parameter sets (δ varying in $[-180°, 180°]$) the experimental event rates were

[1)] Downloadable at: http://www.mpi-hd.mpg.de/personalhomes/globes/glb/0709-nova.html

Table 7.1: Parameters used in simulations, taken from Ref. [34].

Experimental parameter	Value
Baseline	812 km
Expected fiducial mass	14 kt
Source power	0.7 MW
Duration [years]	3ν (1.5ν+$1.5\bar{\nu}$)
Electron energy resolution	$10\%\ \sqrt{E}$
Muon energy resolution	$5\%\ \sqrt{E}$

simulated (neutrino energy spectrum in detectors) and $\Delta\chi^2$, the minimum of χ^2, (Eq. (6.3)) assuming opposite hierarchy was found, i.e. the maximum likelihood estimators of oscillation parameters in the reverse half of parametric space ($\Delta m^2 = -\Delta m^2_{true}$). For the purpose of this procedure solar parameters θ_{12} and Δm^2_{21} are being kept fixed, since their uncertainties are expected to have a minimal impact. Both θ_{13} and $|\Delta m^2|$ were treated with Gaussian priors taking (1σ Gaussian errors) $\sigma(\Delta m^2)/|\Delta m^2| = 6\%$ and $\sigma(\theta_{13})/\theta_{13} = 10\%$ and central values $\Delta m^2 = \pm 2.4 \times 10^{-3}$ eV^2 (NH/IH) and $\sin^2\theta_{13} = 0.023$ (NH), 0.024 (IH) accordingly to their global fits and 2σ errors. The last two oscillation parameters θ_{23} and δ were marginalized over with no priors added using 90% C.L. interval given by MINOS for $\sin^2\theta_{23} \in [0.35, 0.65]$ (taken symmetric) and full range of $\delta \in [-180°, 180°]$.

Figs. 7.1, 7.2 and 7.3 depict the value of $\Delta\chi^2$ as a function of the true δ for both assumed true hierarchies in the case of maximal 23 mixing ($\theta_{23} = 45°$), HO ($\theta_{23} > 45°$) and LO ($\theta_{23} < 45°$) respectively.

7.3 Results

The value of χ^2 represents the agreement of the hypothesis of oscillation parameters with simulated data, the larger χ^2 is, the worse is the congruence of the hypothesis and data (see Section 6.3), or equivalently, the minor is the chance that the hypothesis will be correct, even though it is rejected [38]. This probability is determined by a distribution quantile α corresponding to the value of χ^2, concretely, the probability is $(1 - \alpha)$. In this case, when comparing two normalized histograms of event rates, the quantity χ^2 follows $\boldsymbol{\chi}^2_{(1)}$ distribution, hence, $\chi^2 = 1$ matches the 68% quantile and probability 32%, $\chi^2 = 2.71$ quantile 90% and probability 10%, $\chi^2 = 4$ quantile 95.5% and probability 4.5%, etc.

Summarizing, finding minimal value $\Delta\chi^2$ over a set of oscillation parameters, provided an appropriate mass hierarchy hypothesis, will result in a maximum probability at which the hierarchy hypothesis is valid although it is rejected. Simulated data was always compared with a hypothesis of hierarchy opposite to the true one. Therefore, $\Delta\chi^2 \geq 2.71$ means there is 10% or less chance that the tested hierarchy hypothesis is correct (i.e. it can not explain the observed data well). As the hierarchy can be only normal or inverted, this could be naturally identified as a 90% C.L. for the true hierarchy determination in studies of expected sensitivity to the neutrino mass ordering.

Figs. 7.1, 7.2 and 7.3 show the estimated hierarchy sensitivity at NOνA with 1.5 years of ν and 1.5 years $\bar{\nu}$ data (full lines) and 3 years of ν data only (dashed lines). The favorable NH-LHP-x, IH-UHP-x and unfavorable NH-UHP-x, IH-LHP-x sets of oscillation parameters (see Section 5.6) can be clearly recognized at the first sight and also the fact, that combined $\nu + \bar{\nu}$ data prones to resolve the hierarchy better than ν data only, because it does not suffer from θ_{13} and/or θ_{23} degeneracies.

If NH-LHP and maximal 23-mixing, $\theta_{23} = 45°$, the hierarchy could be resolved at 90% C.L. for $\delta \in [-142°, -40°]$, i.e. for ca 28% of possible δ, see Fig. 7.1. If IH-UHP and $\theta_{23} = 45°$,

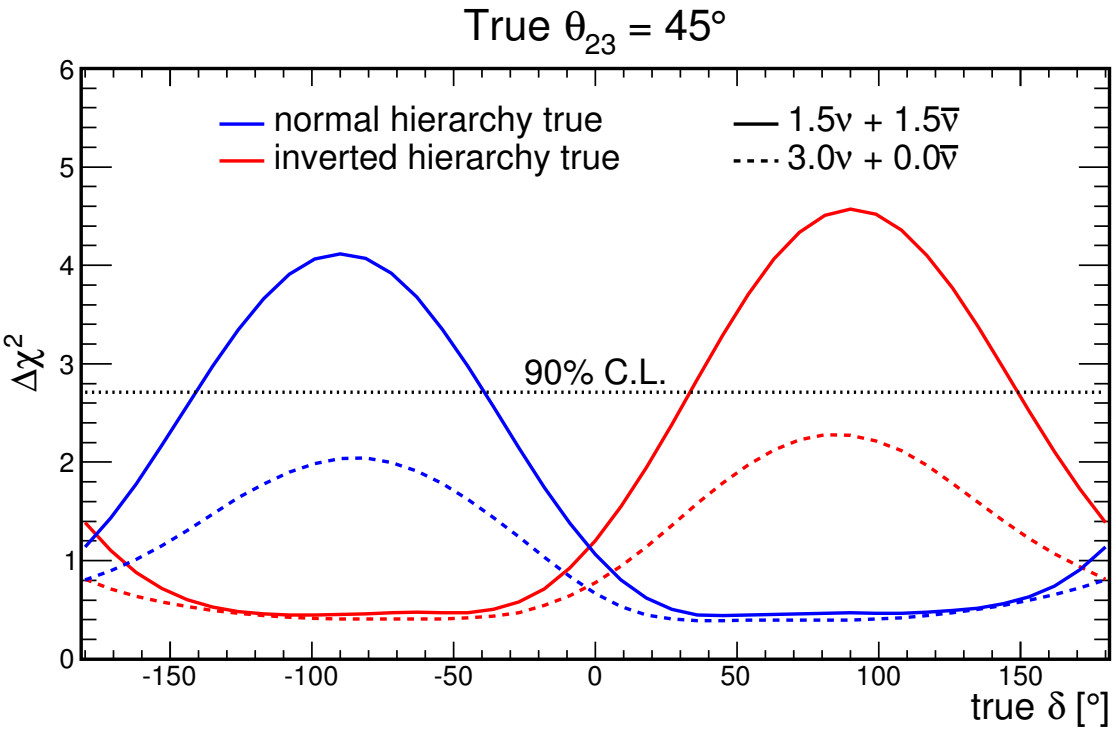

Figure 7.1: $\Delta\chi^2$ (minimal χ^2) for expected hierarchy resolution at NOνA with 3 years ν run (dashed) and 1.5 years ν + 1.5 years $\bar{\nu}$ (full) for true $\sin^2\theta_{23} = 0.5$ assuming 10% uncertainty in θ_{13}, 6% in Δm^2 with central values $\sin^2\theta_{13} = 0.023$ (NH), 0.024 (IH) and $\Delta m^2 = 2.4 \times 10^{-3}$ eV^2. Marginalized over 90% C.L. interval of $\sin^2\theta_{23} \in [0.35, 0.65]$ and $\delta \in [-180°, 180°]$.

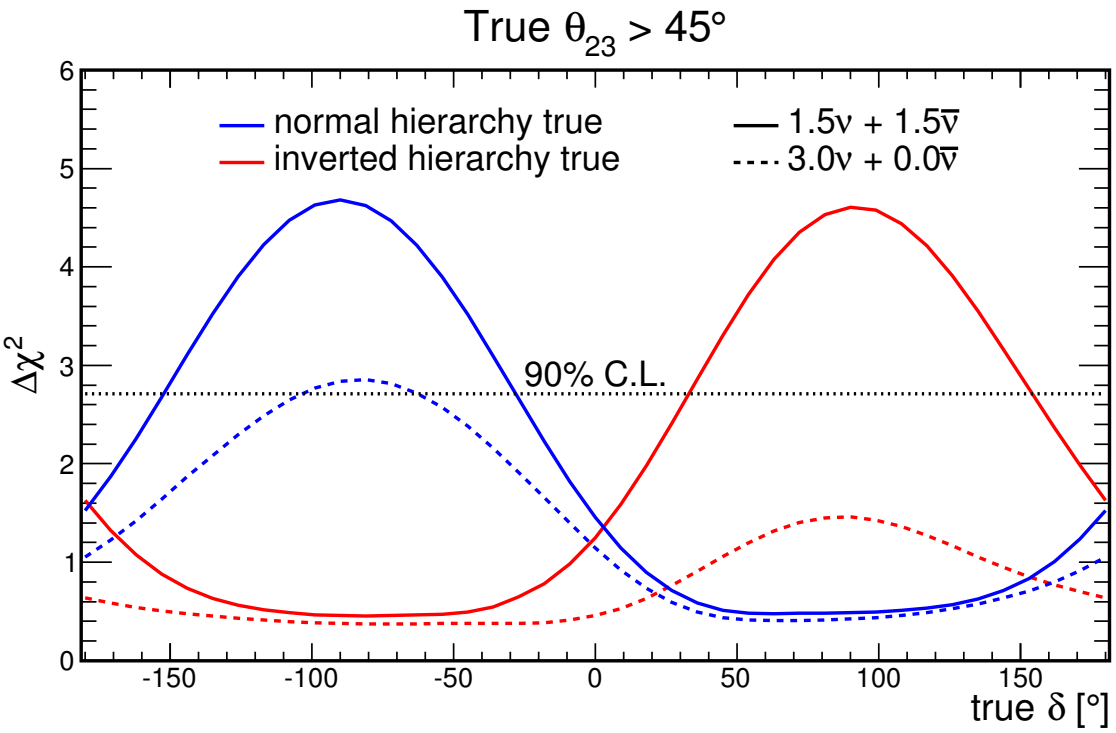

Figure 7.2: $\Delta\chi^2$ (minimal χ^2) for expected hierarchy resolution at NOνA with 3 years ν run (dashed) and 1.5 years ν + 1.5 years $\bar{\nu}$ (full) for true $\sin^2\theta_{23} = 0.56$ (NH), 0.54 (IH) assuming 10% uncertainty in θ_{13}, 6% in Δm^2 with central values $\sin^2\theta_{13} = 0.023$ (NH), 0.024 (IH) and $\Delta m^2 = 2.4 \times 10^{-3}$ eV^2. Marginalized over 90% C.L. interval of $\sin^2\theta_{23} \in [0.35, 0.65]$ and $\delta \in [-180°, 180°]$.

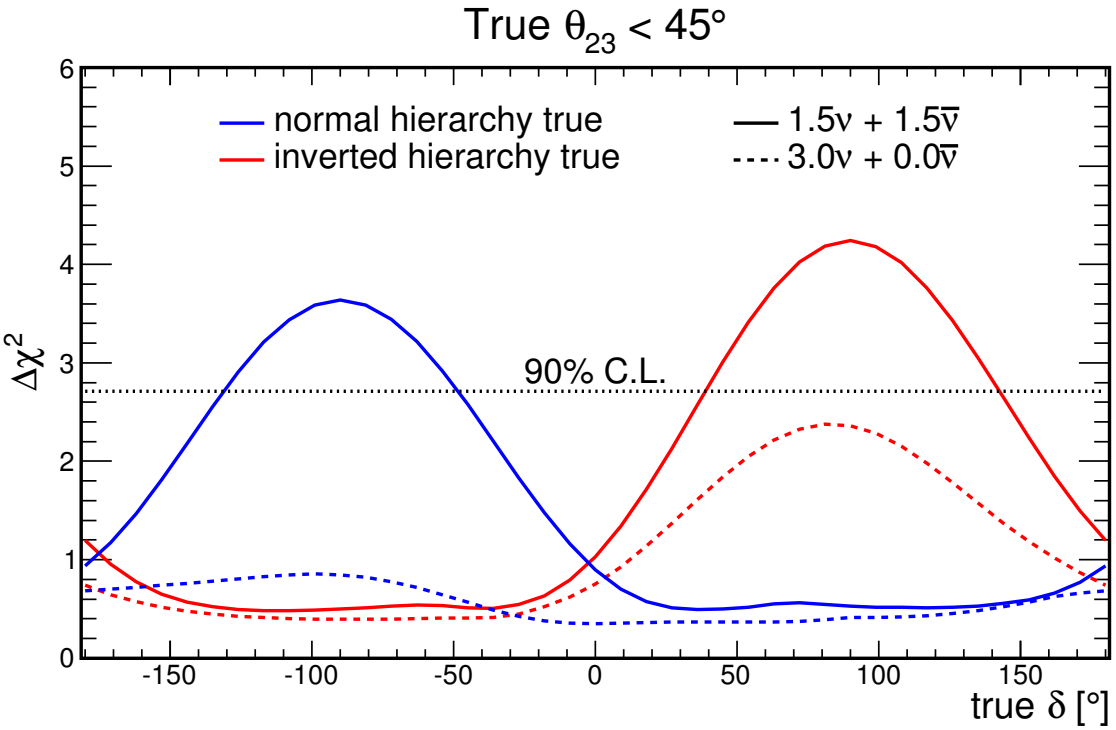

Figure 7.3: $\Delta\chi^2$ (minimal χ^2) for expected hierarchy resolution at NOνA with 3 years ν run (dashed) and 1.5 years ν + 1.5 years $\bar{\nu}$ (full) for true $\sin^2\theta_{23} = 0.44$ (NH), 0.46 (IH) assuming 10% uncertainty in θ_{13}, 6% in Δm^2 with central values $\sin^2\theta_{13} = 0.023$ (NH), 0.024 (IH) and $\Delta m^2 = 2.4 \times 10^{-3}$ eV^2. Marginalized over 90% C.L. interval of $\sin^2\theta_{23} \in [0.35, 0.65]$ and $\delta \in [-180°, 180°]$.

the hierarchy could be resolved for $\delta \in [45°, 150°]$, i.e. for ca 29% of possible δ, also in Fig. 7.1. From Fig. 7.2 the $1.5\nu + 1.5\bar{\nu}$ sensitivities would get improved for $\theta_{23} > 45°$, ca 34% of δ with NH-LHP-HO and ca 33% with IH-UHP-HO. Also, the overall values of $\Delta\chi^2$ are larger in HO, as was predicted. On the other hand, in the case of $\theta_{23} < 45°$, hierarchy could be resolved for ca 24% of possible δ with NH-LHP-LO and ca 28% with IH-UHP-LO, the values of $\Delta\chi^2$ gets smaller, see Fig. 7.3. However, taking pure ν data, $\Delta\chi^2 \geq 2.71$ only with NH-LHP-HO for ca 12% of δ (Fig. 7.2).

Reader can see, that $\Delta\chi^2$ and the ν only sensitivity is quite reduced for IH-UHP-HO and NH-LHP-LO as a whole compared to $\theta_{23} = 45°$, while NH-LHP-HO and IH-UHP-LO is enhanced. This was discussed in Section 5.5 and is caused by the unknown size of θ_{23}, whether and how much it differs from 45°. Generally, θ_{23} being farther from 45° and θ_{13} large enough makes the ν only hierarchy sensitivities such better, that they can be almost as good as $1.5\nu + 1.5\bar{\nu}$ or even better, see Ref. [31]. Nevertheless, this holds only for NH-LHP-HO and IH-UHP-LO with ν data, IH-UHP-HO and NH-LHP-LO are still considerably reduced. The situation would be reversed for $\bar{\nu}$ data: IH-UHP-HO and NH-LHP-LO improved, while NH-LHP-HO and IH-UHP-LO reduced.

The only degeneracy not to be removed by acquiring $\bar{\nu}$ information on oscillations is the one caused by unfavorable values of δ. More precise knowledge of θ_{13} and θ_{23}, provided θ_{13} is large enough, and consequent narrowing of oscillation parametric space leads to a weakening of the parameters correlations and generally better resolution to the mass hierarchy, but significantly for pure $\nu/\bar{\nu}$ data. Unfortunately, this is possible only in NH-LHP-HO and IH-UHP-LO (ν data), or IH-UHP-HO and NH-LHP-LO ($\bar{\nu}$ data) scenarios. Reader shall note, that NOνA itself (and, obviously, in a cooperation with other oscillation experiments) has an ability to further specify all the parameters θ_{13}, θ_{23}, δ and Δm^2 and put tighter limits on their experimental errors. Therefore, the final sensitivity could sustain

appreciable improvement (in the sense it cannot get worse, provided no measurements in a strong disagreement with recent parameter estimates occur). An earlier NOνA $\bar{\nu}$ run can bring the first results upon the mass hierarchy problem sooner and thereby can set the future aims and could help to optimize NOνA and planned experiments (LBNF/DUNE mainly) in order to use them more effectively and efficiently in neutrino mass hierarchy (and CP violation) search.

8. Conclusion

The standard formalism and three neutrinos model of neutrino oscillations including vaccum propagation and oscillation probabilities were introduced. Experimental foundations in oscillation parameters search were discussed and recent status of these parameters was presented.

The NOνA long-baseline neutrino oscillation experiment and its main features, i.e. NuMI beamline, off-axis concept and detectors, were described.

The effects of matter in neutrino oscillations were studied. Effective scattering potentials and matter Hamiltonian were derived. An approximative diagonalization of the matter Hamiltonian was performed, using consecutive rotations, resulting in new effective oscillation parameters in matter. Because of their later utilization in mass hierarchy determination, the so-called matter resonances were especially focused at:

1. There is a substantive difference between ν and $\bar{\nu}$ oscillations in a medium due to its inherent CP assymetry, i.e. extrinsic CP violation of neutrino oscillations.
2. The resonance behavior of $\nu/\bar{\nu}$ oscillations depends on the sign(s) of Δm^2_{ij}. The position of 13-resonance (in ν or $\bar{\nu}$ sector) is connected to the realized normal or inverted mass hierarchy of neutrinos in particular.
3. The presence or absence of the matter resonance effectively enhances or attenuates the oscillation probabilities in corresponding oscillation appearance and disappearance channels compared to the vacuum case.

Aiming at $\nu_\mu \to \nu_e$ channel the main principle of determining the neutrino mass hierarchy, i.e. the sign of Δm^2, with long-baseline accelerator experiments was explained. By computing $P(\nu_\mu \to \nu_e)$ and/or $P(\bar{\nu}_\mu \to \bar{\nu}_e)$ several issues were deduced:

1. Currently active long-baseline experiments are able to resolve the mass hierarchy depending on the true value of δ only in favorable scenarios: NH-LHP and IH-UHP.
2. There are 3 considerable degeneracies in the mass hierarchy problem allowed by recent estimates of oscillation parameters: θ_{13}, θ_{23} and δ.
3. δ degeneracy is always present due to the unknown (not precise enough) size of δ.
4. A combination of $\nu + \bar{\nu}$ data can withdraw the θ_{13} and θ_{23} degeneracies. Hence, it is vital to investigate both $\nu_\mu \to \nu_e$ and $\bar{\nu}_\mu \to \bar{\nu}_e$ oscillations.

With an aid of GLoBES software the possibility of mass hierarchy determination at NOνA was analyzed, the advantage of an early $\bar{\nu}$ run in detail:

1. An earlier $\bar{\nu}$ run of NOνA could bring noticeable results in the mass hierarchy question much sooner than 3 years ν + 3 years $\bar{\nu}$ initially scheduled.
2. 1.5 years ν + 1.5 years $\bar{\nu}$ of data taking can reject the wrong hierarchy at 90% C.L. for estimated $24 - 34\%$ of possible δ depending on the sizes of θ_{13} and θ_{23}.

References

[1] Carlo Giunti and Chung W. Kim. *Fundamentals of Neutrino Physics and Astrophysics*. Oxford University Press, 2007.

[2] K. Zuber. *Neutrino Physics*. Series in High Energy Physics, Cosmology and Gravitation Series. Taylor & Francis, 2004.

[3] K.A. Olive et al. Review of Particle Physics. *Chin.Phys.*, C38:090001, 2014.

[4] J.A. Thomas and P.L. Vahle. *Neutrino oscillations: Present Status and Future Plans*. World Scientific, 2008.

[5] Boris Kayser. Neutrino Oscillation Phenomenology. 2008, arXiv:0804.1121.

[6] Boris Kayser. Neutrino Oscillation Physics. 2012, arXiv:1206.4325.

[7] Boris Kayser. Neutrino physics. *eConf*, C040802:L004, 2004, hep-ph/0506165.

[8] Evgeny K. Akhmedov. Neutrino oscillations: Theory and phenomenology. *Nucl.Phys.Proc.Suppl.*, 221:19–25, 2011, hep-ph/0610064.

[9] Carlo Giunti and Marco Laveder. Neutrino mixing. 2003, hep-ph/0310238.

[10] V. Antonelli, L. Miramonti, C. Peña Garay, and A. Serenelli. Solar Neutrinos. *Advances in High Energy Physics*, 2013(351926), 2013, doi:10.1155/2013/351926.

[11] Takaaki Kajita. Atmospheric neutrinos. *Adv.High Energy Phys.*, 2012(504715), 2012, doi:10.1155/2012/504715.

[12] G. J. Feldman, J. Hartnell, and T. Kobayashi. Long-Baseline Neutrino Experiments. *Advances in High Energy Physics*, 2013(475749), 2013, doi:10.1155/2013/475749.

[13] Hiroshi Nunokawa, Stephen J. Parke, and Jose W.F. Valle. CP Violation and Neutrino Oscillations. *Prog.Part.Nucl.Phys.*, 60:338–402, 2008, arXiv:0710.0554.

[14] Mattias Blennow and Alexei Yu. Smirnov. Neutrino Propagation in Matter. *Advances in High Energy Physics*, 2013(972485), 2013, doi:10.1155/2013/972485, arXiv:1306.2903.

[15] C. Adams et al. The Long-Baseline Neutrino Experiment: Exploring Fundamental Symmetries of the Universe. 2013, arXiv:1307.7335.

[16] Evgeny K. Akhmedov. Matter effects in oscillations of neutrinos traveling short distances in matter. *Phys.Lett.*, B503:133–139, 2001, doi:10.1016/S0370-2693(01)00165-4, hep-ph/0011136.

[17] Chao Zhang. Recent Results From The Daya Bay Experiment. 2015, arXiv:1501.04991.

[18] Alexandre Sousa. First MINOS+ Data and New Results from MINOS. 2015, arXiv:1502.07715.

[19] Martin David Haigh. Results from T2K. 2015, arXiv:1501.04283.

[20] NOνA Collaboration. Proposal to Build a 30 Kiloton Off-Axis Detector to Study $\nu_\mu \to \nu_e$ Oscillations in the NuMI Beamline. NOVA-doc-593-v1, 2005, 2015/02/16.

[21] D. S. Ayres et al. NOνA Technical Design Report. FERMILAB-DESIGN-2007-01, 2007, 2015/02/16.

[22] J. M. Paley. Status of the NOνA Experiment, NOVA-doc-11714-v1, 2014, presented in Quy Nhon, Vietnam, 2014/07/31.

[23] G. J. Feldman. NOνA Experiment: Preparations for Data Taking, NOVA-doc-9245-v1, 2013, presented at Fermilab PAC, USA, 2013/06/05.

[24] C. Backhouse. Results from MINOS and NOvA. 2015, arXiv:1501.01016.

[25] Mattias Blennow. Matter and damping effects in neutrino mixing and oscillations. 2005, AlbaNova University, Royal Institute of Technology, Stockholm, Sweden, licentiate thesis, http://theophys.kth.se/∼mbl/licthesis.ps.

[26] Martin Freund. Analytic approximations for three neutrino oscillation parameters and probabilities in matter. *Phys.Rev.*, D64:053003, 2001, hep-ph/0103300.

[27] S. K. Agarwalla, Y. Kao, and T. Takeuchi. Analytical approximation of the neutrino oscillation matter effects at large θ_{13}. *JHEP*, 1404:047, 2014, arXiv:1302.6773.

[28] A. Bueno, Mario Campanelli, and A. Rubbia. Physics potential at a neutrino factory: Can we benefit from more than just detecting muons? *Nucl.Phys.*, B589:577–608, 2000, hep-ph/0005007.

[29] H.W. Zaglauer and K.H. Schwarzer. The Mixing Angles in Matter for Three Generations of Neutrinos and the MSW Mechanism. *Z.Phys.*, C40:273, 1988, doi:10.1007/BF01555889.

[30] Tommy Ohlsson and Shun Zhou. Extrinsic and Intrinsic CPT Asymmetries in Neutrino Oscillations. *Nucl.Phys.*, B893:482–500, 2015, arXiv:1408.4722.

[31] Suprabh Prakash, Ushak Rahaman, and S. Uma Sankar. The need for an early anti-neutrino run of NOνA. *JHEP*, 1407:070, 2014, arXiv:1306.4125.

[32] K.N. Deepthi, C. Soumya, and R. Mohanta. Revisiting the sensitivity studies for leptonic CP-violation and mass hierarchy with T2K, NOνA and LBNE experiments. *New J.Phys.*, 17(2):023035, 2015, arXiv:1409.2343.

[33] C. Soumya, K.N. Deepthi, and R. Mohanta. A comprehensive study of the discovery potential of NOvA, T2K and T2HK experiments and the effect of cross-section uncertainty. 2014, arXiv:1408.6071.

[34] P. Huber, J. Kopp, M. Lindner, M. Rolinec, and W. Winter. GLoBES general long baseline experiment simulator: User's and experiment definition manual. 2010, http://www.mpi-hd.mpg.de/personalhomes/globes/documentation/globes-manual-3.0.8.pdf, 2015/03/07.

[35] P. Huber, M. Lindner, and W. Winter. Simulation of long-baseline neutrino oscillation experiments with GLoBES (General Long Baseline Experiment Simulator). *Comput.Phys.Commun.*, 167:195, 2005, hep-ph/0407333.

[36] P. Huber, J. Kopp, M. Lindner, M. Rolinec, and W. Winter. New features in the simulation of neutrino oscillation experiments with GLoBES 3.0: General Long Baseline Experiment Simulator. *Comput.Phys.Commun.*, 177:432–438, 2007, hep-ph/0701187.

[37] Glen Cowan. Goodness of fit and wilks' theorem. 2013, http://wwwusers.ts.infn.it/∼milotti/Didattica/StatisticaAvanzata/Cowan_2013.pdf, 2015/03/30.

[38] Glen Cowan, Kyle Cranmer, Eilam Gross, and Ofer Vitells. Asymptotic formulae for likelihood-based tests of new physics. *Eur.Phys.J.*, C71:1554, 2011, arXiv:1007.1727.

[39] Jiří Anděl. *Matematická statistika.* SNTL & Alfa, 1985.

[40] Radhakrishna Calyampudi Rao. *Lineární metody statistické indukce a jejich aplikace.* Academia, translation J. Machek, 1978.

[41] K. Nishikawa et al. Tokai-to-Kamioka (T2K) Long Baseline Neutrino Oscillation Experiment Proposal. 2006, http://j-parc.jp/researcher/Hadron/en/pac_0606/pdf/p11-Nishikawa.pdf, 2015/03/21.

[42] Mattias Blennow and Thomas Schwetz. Indentifying the Neutrino mass Ordering with INO and NOνA. 2012, arXiv:1203.3388.

[43] R.B. Patterson. The NOνA Experiment: Status and Outlook. 2012, arXiv:1209.0716.

[44] Jonathan M. Paley. NOνA Collaboration, LBNE Collaboratoin. The search for CP violation and the determination of the neutrino mass hierarchy in NOνA and LBNE. *PoS*, ICHEP2012:393, 2013.

[45] K. Abe et al. Neutrino Oscillation Physics Potential of the T2K Experiment. *PTEP*, 2015(4):043C01, 2014, arXiv:1409.7469.

[46] E. A. Paschos and J. Y. Yu. Neutrino interactions in oscillation experiments. *Phys. Rev.*, D65:033002, 2002, hep-ph/0107261.

List of Tables

List of Figures

List of Abbreviations & Acronyms

CPT	Charge-Parity-Time
C.L.	Confidence Level
NOνA	NuMI Off-axis ν_e Appearance experiment
LBNE	Long Baseline Neutrino Experiment
LBNF	Long Baseline Neutrino Facility
DUNE	Deep Underground Neutrino Experiment
NuMI	Neutrinos at the Main Injector
K2K	KEK To Kamioka experiment
KEK	Kō Enerugī Kasokuki Kenkyū Kikō (High Energy Accelerator Research Organization)
T2K	Tokai To Kamioka experiment
OPERA	Oscillation Project with Emulsion-tRacking Apparatus
SPS	Super Proton Synchrotron
CNGS	CERN Neutrinos to Gran Sasso
CERN	Conseil Européen pour la Recherche Nucléaire (European Organization for Nuclear Research)
MINOS	Main Injector Neutrino Oscillation Search
LSND	Liquid Scintillator Neutrino Detector
KARMEN	KArlsruhe Rutherford Medium Energy Neutrino experiment
SNO	Sudbury Neutrino Observatory
SAGE	Soviet–American Gallium Experiment
GALLEX	GALLium EXperiment
RENO	Reactor Experiment for Neutrino Oscillations
SSM	Standard Solar Model
SM	Standard Model
CC	Charged Current
NC	Neutral Current
ND	Near Detector
FD	Far Detector
NDOS	Near Detector On the Surface
APD	Avalanche PhotoDiode
POT	Protons On Target
MSW	Mikheev-Smirnov-Wolfenstein
GLoBES	General Long Baseline Experiment Simulator
AEDL	Abstract Experiment Definition Language
NH	Normal Hierarchy
IH	Inverted Hierarchy
UHP	Upper Hyper-Plane ($\delta \in [0, 180°]$)
LHP	Lower Hyper-Plane ($\delta \in [-180°, 0]$)
HO	Higher Octant ($\theta_{23} > 45°$)
LO	Lower Octant ($\theta_{23} < 45°$)

Notation

$\nu, \bar{\nu}$	neutrino and antineutrino
p, n	proton and neutron, observed nucleons
e, μ, τ	electron, muon and tauon, observed charged leptons
ν_e, ν_μ, ν_τ	electron, muon and tauon neutrino, observed neutral leptons
$i, j, k \ldots$	denotation of mass eigenstates
$\alpha, \beta, \gamma \ldots$	denotation of flavor eigenstates
$\|\nu_\alpha\rangle$	flavor eigenstate of neutrino
$\|\nu_i\rangle$	mass eigenstate of neutrino
$\|N_i\rangle$	effective mass eigenstate of neutrino in matter
ν_f	neutrino vector in the flavor representation, coordinates in $\|\nu_\alpha\rangle$ basis
ν_m	neutrino vector in the mass representation, coordinates in $\|\nu_i\rangle$ basis
m_i	mass of neutrino mass eigenstate
M_i	effective mass of neutrino mass eigenstate in matter
$\Delta m^2_{ij} = m^2_i - m^2_j$	squared-mass splittings
θ_{ij}	mixing angles
Θ_{ij}	effective mixing angles in matter
δ	the Dirac phase
δ_{ij}	Kronecker symbol
a, b	Majorana phases
U	mixing matrix
$U_{\alpha i}$	elements of mixing matrix
$\mathcal{U}$	effective mixing matrix in matter
H	free or vacuum Hamiltonian
$\mathcal{H}$	effective matter Hamiltonian
E	energy
p	momentum
t	time
x	space coordinate, position
L	baseline or travelling distance
$\mathrm{Amp}(\cdot)$	amplitude of a particular process
$P(\nu_\alpha \to \nu_\beta)$	oscillation probability from a flavor α to β, appearance probability of ν_β for initial ν_α
$\langle \cdot \| \cdot \rangle$	inner product
V	interaction potential
G_F	Fermi coupling constant
N_e, N_n	electron and nucleon density
$\Re\mathfrak{e}, \Im\mathfrak{m}$	real and imaginary part of a complex number
*	complex conjugate
†	hermitian conjugate
^{T}	transposition
$L(\cdot)$	likelihood function
$\boldsymbol{\chi}^2_{(N)}$	chi-square distribution with N degrees of freedom